



**HAL**  
open science

# Effect of Diffraction on Wigner Distributions of Optical Fields and how to Use It in Optical Resonator Theory. III -Ray Tracing in Resonators

Pierre Pellat-Finet, Éric Fogret

► **To cite this version:**

Pierre Pellat-Finet, Éric Fogret. Effect of Diffraction on Wigner Distributions of Optical Fields and how to Use It in Optical Resonator Theory. III -Ray Tracing in Resonators. 2022. hal-03628456

**HAL Id: hal-03628456**

**<https://hal.science/hal-03628456>**

Preprint submitted on 2 Apr 2022

**HAL** is a multi-disciplinary open access archive for the deposit and dissemination of scientific research documents, whether they are published or not. The documents may come from teaching and research institutions in France or abroad, or from public or private research centers.

L'archive ouverte pluridisciplinaire **HAL**, est destinée au dépôt et à la diffusion de documents scientifiques de niveau recherche, publiés ou non, émanant des établissements d'enseignement et de recherche français ou étrangers, des laboratoires publics ou privés.

# Effect of Diffraction on Wigner Distributions of Optical Fields and how to Use It in Optical Resonator Theory.

## III – Ray Tracing in Resonators

**Pierre Pellat-Finet and Éric Fogret**

*Laboratoire de Mathématiques de Bretagne Atlantique UMR CNRS 6205  
Université de Bretagne Sud, B. P. 92116, 56321 Lorient cedex, France*

---

**Abstract.** The third part of the paper is devoted to ray tracing in optical resonators. The employed method for dealing with the issue uses the elliptical or hyperbolic rotations that Wigner distributions associated with optical fields undergo during propagation from one spherical mirror of a resonator to the other. It is illustrated by various examples concerning meridional or skew rays, reentrant in stable resonators or propagating in unstable resonators. A classification of optical resonators is eventually deduced.

**Keywords:** Fourier optics, fractional-order Fourier transformation, optical resonators, ray tracing, reentrant rays, skew rays, Wigner distribution.

**PACS:** 42.30.Kq

### Content

1. Introduction .....	1
2. General ray tracing .....	2
3. Reentrant rays in stable resonators .....	7
4. Tracing reentrant meridional rays in stable resonators .....	10
5. Reentrant skew rays in stable resonators .....	18
6. Ray tracing in unstable resonators .....	24
7. Conclusion .....	31
References .....	32

---

## 1 Introduction

Ray tracing, which is widely used in the design of optical systems, such as lenses, objective lenses and optical instruments, some of which forming optical images, is implemented by applying the fundamental laws of geometric optics, such as Snell's law, and makes it possible to quantify the effects of aberrations (both geometrical and chromatic). A light ray is generally determined by its height, relative to a reference plane, and the angle it makes with a straight line parallel to the optical axis. A ray translation in free space from a (refracting or reflective) surface to another one is analyzed according to a direct geometrical formulation, which links the ray-heights relative to two reference planes, tangent to the previous surfaces.

We introduce here an alternative method of ray tracing, in which ray translations are analyzed in the framework of a scalar theory of diffraction, by means of the representations of optical fields by their associated Wigner distributions [1–3], and which results from the identification of two quantities: on the one hand, the pair made up of a point on a ray and the ray direction of propagation; on the other hand, the pair made up of a point in a given optical field and a spatial frequency. The advantage of proceeding in this way is to treat skew rays as easily as meridional ones. The method is applied to ray tracing in optical resonators.

---

pierre.pellat-finet@univ-ubs.fr, eric.fogret@univ-ubs.fr

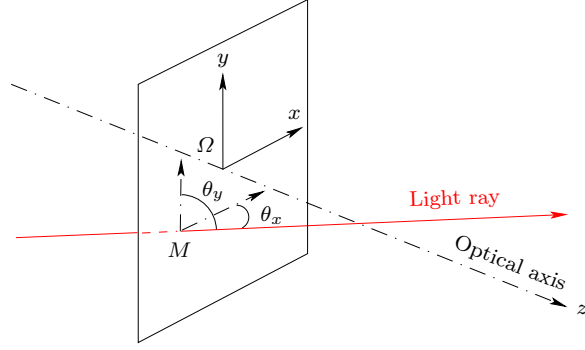


Figure 1: A light ray is usually defined by the Cartesian coordinates  $x$  and  $y$  of the point  $M$  where it pierces a given plane, and by the direction cosines  $\cos\theta_x$  and  $\cos\theta_y$ . In the present work, the plane is replaced by a spherical cap.

Given a plane orthogonal to the axis of an optical centred system, a straight light ray is characterized by the point where it pierces the plane and by the direction along which it propagates. The previous point, say  $M$ , is represented by its Cartesian coordinates  $x$  and  $y$  in the plane, that is, by the vector  $\Omega M = \mathbf{r} = (x, y)$ , where  $\Omega$  is the coordinate origin; and the propagation direction by the direction cosines  $\alpha = \cos\theta_x$  and  $\beta = \cos\theta_y$  (Fig. 1), which form a vector, denoted  $\Phi = (\alpha, \beta)$  (the corresponding vector-space is the angular-frequency space—“frequency” being understood as “spatial frequency”). A light ray is eventually represented by  $(\mathbf{r}, \Phi)$ .

The preceding representation of a light ray is extended, in the present article, by replacing the plane by a spherical cap (centred on the optical axis). A light ray will still be represented by  $(\mathbf{r}, \Phi)$ , where  $\mathbf{r}$  and  $\Phi$  will be appropriately defined.

In Fourier optics, the vector  $\mathbf{r}$  is the variable used to describe the optical field amplitude, and  $\Phi$  to describe the (spherical) angular spectrum, related to the two-dimensional Fourier transform of the field amplitude. Consequently,  $(\mathbf{r}, \Phi)$  corresponds to a space–frequency representation of the optical field (where “frequency” means “spatial frequency”).

In the first two parts of the paper [1, 2], we introduced a 4–dimensional scaled phase-space, in which coordinates were scaled versions of  $\mathbf{r}$  and  $\Phi$ , so that a point in the scaled phase-space represents a light ray. The scaled phase-space is equipped with an Euclidean structure, giving meaning to rotations operating on it. A Wigner distribution, which represents a given optical field, both in space and frequency in the scaled phase-space, may then be seen as a set of light rays associated with the optical field. Knowing how Wigner distributions are transformed along propagation through an optical system leads to describe how light rays propagate through the system. That constitutes the principle of the ray-tracing method developed in the present paper and focused on ray propagation in optical resonators.

## 2 General ray tracing

### 2.1 Physical parameters

We recall that a point  $M$  on a spherical cap  $\mathcal{A}$  is spotted by the coordinates of its (orthogonal) projection  $m$  on the plane  $\mathcal{P}$ , tangent to  $\mathcal{A}$  at its vertex  $\Omega$  (Fig. 2). With Cartesian coordinates  $x$  and  $y$ , the point  $M$  is represented by the vector  $\mathbf{r} = \Omega m$ . That is only a way of spotting  $M$ , and vectors  $\Omega M$  and  $\mathbf{r} = \Omega m$  should not be confused.

We denote  $z$  the direction of propagation and choose unit vectors  $\mathbf{e}_x$ ,  $\mathbf{e}_y$  and  $\mathbf{e}_z$  along directions  $x$ ,  $y$  and  $z$ . The basis  $(\mathbf{e}_x, \mathbf{e}_y, \mathbf{e}_z)$  is a direct orthogonal basis:  $\mathbf{e}_z = \mathbf{e}_x \times \mathbf{e}_y$  ( $\times$  denotes the vector product).

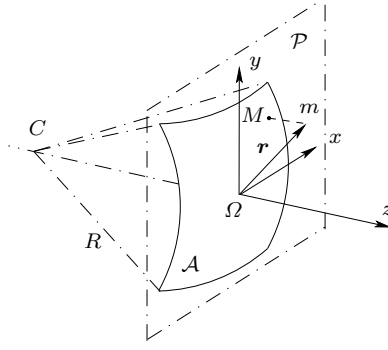


Figure 2: Cartesian coordinates on a spherical cap  $\mathcal{A}$ . Point  $m$  is the orthogonal projection of  $M$  onto the tangent plane  $\mathcal{P}$  at  $\Omega$  (the vertex of  $\mathcal{A}$ ). The curvature center of  $\mathcal{A}$  is  $C$ , its curvature radius is  $R = \overline{\Omega C}$ .

We consider the unit vector  $\mathbf{e}_n$  normal to  $\mathcal{A}$  at  $M$  and such that  $\mathbf{e}_n \cdot \mathbf{e}_z > 0$  (the central dot denotes the Euclidean scalar product of vectors). We introduce the following unit vectors (Fig. 3)

$$\mathbf{e}_\xi = \frac{\mathbf{e}_y \times \mathbf{e}_n}{\|\mathbf{e}_y \times \mathbf{e}_n\|}, \quad \text{and} \quad \mathbf{e}_\eta = \frac{\mathbf{e}_n \times \mathbf{e}_x}{\|\mathbf{e}_n \times \mathbf{e}_x\|}. \quad (1)$$

Vectors  $\mathbf{e}_\xi$  and  $\mathbf{e}_\eta$  lie in the plane  $\mathcal{T}$ , tangent to  $\mathcal{A}$  at  $M$ , and the basis  $(\mathbf{e}_n, \mathbf{e}_\xi, \mathbf{e}_\eta)$  is a direct basis:  $\mathbf{e}_n = \mathbf{e}_\xi \times \mathbf{e}_\eta$ .

A light ray passing by  $M$  is along a unit vector  $\mathbf{e}_u$  and we denote  $\theta_\xi$ ,  $\theta_\eta$  and  $\theta_n$  the angles between  $\mathbf{e}_u$  and vectors  $\mathbf{e}_\xi$ ,  $\mathbf{e}_\eta$  and  $\mathbf{e}_n$  (Fig. 3). (If necessary, angles are taken from the axis vectors toward  $\mathbf{e}_u$ ; for example  $\theta_n$  is the angle from  $\mathbf{e}_n$  toward  $\mathbf{e}_u$ .) The corresponding direction cosines are

$$\xi = \cos \theta_\xi = \mathbf{e}_\xi \cdot \mathbf{e}_u, \quad \eta = \cos \theta_\eta = \mathbf{e}_\eta \cdot \mathbf{e}_u, \quad \zeta = \cos \theta_n = \mathbf{e}_n \cdot \mathbf{e}_u. \quad (2)$$

Since  $\mathbf{e}_u$  is a unit vector, we have  $\xi^2 + \eta^2 + \zeta^2 = 1$ , and  $\mathbf{e}_u$  is perfectly defined by  $\xi$  and  $\eta$  (once given the sense of propagation).

The angular-frequency vector, associated with the considered ray, is

$$\Phi = (\xi, \eta), \quad (3)$$

and is the projection of vector  $\mathbf{e}_u$  onto the plane tangent to  $\mathcal{A}$  at  $M$ . It is such that

$$\|\Phi\| = |\sin \theta_n|. \quad (4)$$

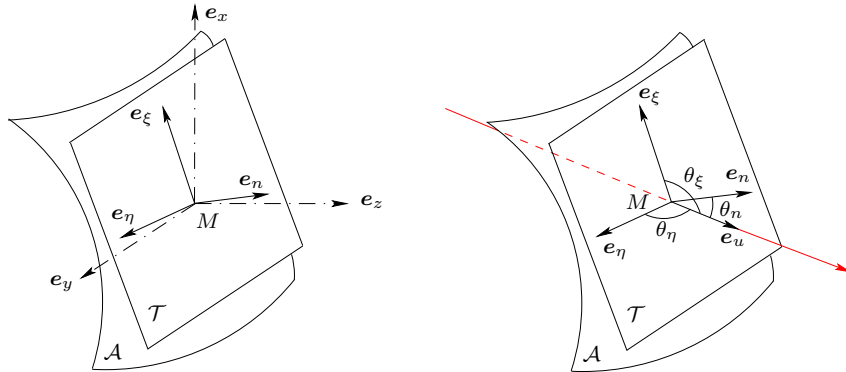


Figure 3: Left: definition of an orthogonal basis at  $M$ ; vector  $\mathbf{e}_n$  is orthogonal to  $\mathcal{A}$  at  $M$ , and  $\mathbf{e}_z \cdot \mathbf{e}_n > 0$ . Right: the unit vector  $\mathbf{e}_u$  is along the light ray at  $M$ , and its direction cosines are  $\cos \theta_\xi$ ,  $\cos \theta_\eta$  and  $\cos \theta_n$ .

Finally we remark that the previous ray, which intercepts  $\mathcal{A}$  at  $M$ , is perfectly defined by the ordered pair  $(\mathbf{r}, \boldsymbol{\Phi})$ .

## 2.2 Ray tracing from one spherical cap to another

The issue of ray tracing can be expressed as follows. Given two spherical caps  $\mathcal{A}$  and  $\mathcal{A}'$ , with a common axis  $z$ , and given a ray  $(\mathbf{r}, \boldsymbol{\Phi})$  on  $\mathcal{A}$ , find the corresponding ray  $(\mathbf{r}', \boldsymbol{\Phi}')$  on  $\mathcal{A}'$  (Fig. 4).

In the expression  $(\mathbf{r}', \boldsymbol{\Phi}')$ , we have  $\mathbf{r}' = (x', y')$ , where  $x'$  and  $y'$  are the coordinates of  $M'$ , the point where the ray pierces cap  $\mathcal{A}'$ . Although the direction of the ray is the same at  $M$  and at  $M'$ , generally  $\boldsymbol{\Phi}' \neq \boldsymbol{\Phi}$ , because  $\boldsymbol{\Phi}$  refers to the normal to  $\mathcal{A}$  at  $M$ , and  $\boldsymbol{\Phi}'$  to the normal to  $\mathcal{A}'$  at  $M'$ . More precisely, let  $\theta_n$  be the angle between  $\mathbf{e}_n$  and  $\mathbf{e}_u$ , that is, between the normal to  $\mathcal{A}$  at  $M$  and the ray; and let  $\theta'_n$  be the angle between  $\mathbf{e}'_n$  and  $\mathbf{e}_u$ , that is, between the normal to  $\mathcal{A}'$  at  $M'$  and the ray. In general  $\theta_n \neq \theta'_n$ , so that  $\|\boldsymbol{\Phi}\| = |\sin \theta_n| \neq |\sin \theta'_n| = \|\boldsymbol{\Phi}'\|$ .

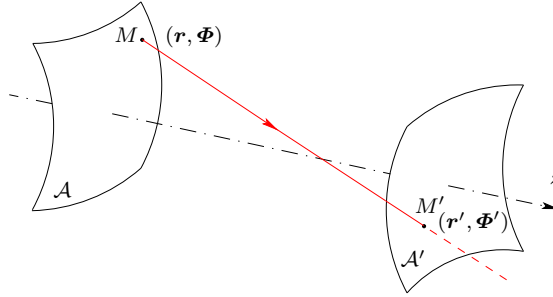


Figure 4: Ray tracing from a spherical cap  $\mathcal{A}$  to another spherical cap  $\mathcal{A}'$ : given  $(\mathbf{r}, \boldsymbol{\Phi})$ , find  $(\mathbf{r}', \boldsymbol{\Phi}')$ .

## 2.3 Refractive surface: Snell's law

Ray tracing also involves rays passing through a refracting surface  $\mathcal{D}$ , separating two homogeneous media with respective refractive index  $n$  and  $n'$  (Fig. 5). For a given ray, incident at a point  $M$ , Snell's law is twofold:

1. The incident and the refracted rays lie in the plane of incidence.
2. The incident angle  $\theta_n$  and the refraction angle  $\theta'_n$  are such that  $n \sin \theta_n = n' \sin \theta'_n$ .

Angles  $\theta_n$  (incidence) and  $\theta'_n$  (refraction) are taken from the normal toward the ray: they have the same sign (see Fig. 5). Since the plane of incidence contains the normal to the refracting surface at  $M$ , the first item above implies that  $\boldsymbol{\Phi}$  and  $\boldsymbol{\Phi}'$  are collinear (because they are respective

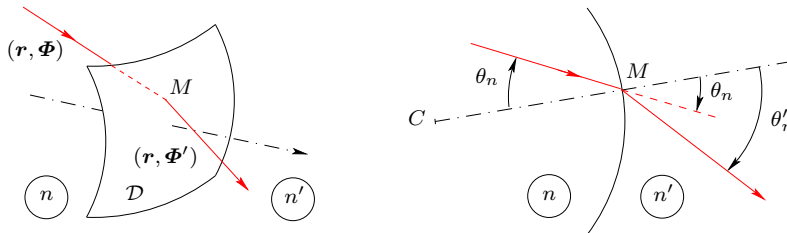


Figure 5: Left: ray tracing through a refracting sphere  $\mathcal{D}$  (Snell's law). Right: diagram in the plane of incidence;  $C$  is the curvature center of the sphere, and angles are taken from the normal at  $M$  toward the ray.

orthogonal projections of the unit vectors  $\mathbf{e}_u$  and  $\mathbf{e}'_u$ ). The second item yields  $n\|\boldsymbol{\Phi}\| = n'\|\boldsymbol{\Phi}'\|$ . Finally, Snell's law is expressed by

$$n\boldsymbol{\Phi} = n'\boldsymbol{\Phi}'. \quad (5)$$

Since the point  $M$  is common to both the incident and the refracted rays, we have

$$(\mathbf{r}', \boldsymbol{\Phi}') = \left( \mathbf{r}, \frac{n}{n'} \boldsymbol{\Phi} \right). \quad (6)$$

Equation (6) is a complete form of Snell's law (refraction). It holds true for screw as well as for meridional rays.

## 2.4 Reflection on a spherical mirror

Consider a ray  $(\mathbf{r}, \boldsymbol{\Phi})$  incident at point  $M$  on a mirror (Fig. 6). The reflected ray is  $(\mathbf{r}', \boldsymbol{\Phi}')$ . The direction of propagation  $z$  is changed into  $z'$  after reflection, and  $z'$  is opposite to  $z$ ; according to our convention (see Sect. 2.1), that means that the normal vectors at  $M$  (before and after reflection) are opposite:  $\mathbf{e}'_n = -\mathbf{e}_n$ . Thus the incidence angle  $\theta_n$  between  $\mathbf{e}_n$  and the (prolonged) incident ray is also the angle between  $\mathbf{e}'_n$  and the incident ray, as it is usually defined in optics (see Fig. 6). The reflection angle  $\theta'_n$  is opposite to the incidence angle  $\theta_n$  (they are both taken from the normal toward the ray). If we maintain axes  $x$  and  $y$  after reflection (namely  $x' = x$  and  $y' = y$ ), we obtain  $\boldsymbol{\Phi} = \boldsymbol{\Phi}'$ , and  $\mathbf{r}' = \mathbf{r}$ . Finally, we have  $(\mathbf{r}', \boldsymbol{\Phi}') = (\mathbf{r}, \boldsymbol{\Phi})$ .

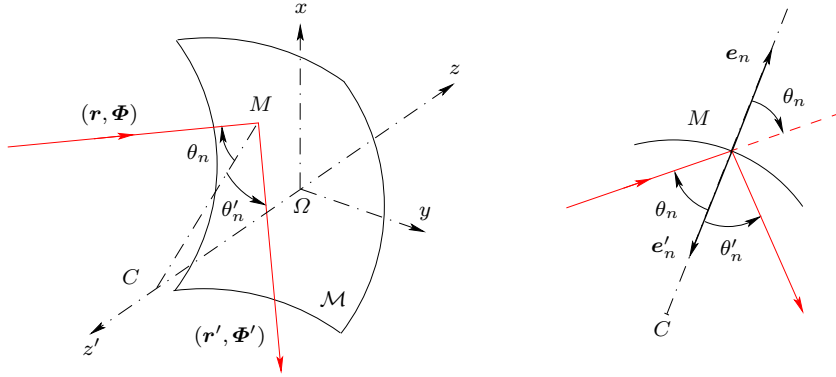


Figure 6: Left: ray tracing for reflection on a spherical mirror  $\mathcal{M}$ . Right: diagram in the plane of incidence ( $C$  is the mirror curvature center).

## 2.5 Ray tracing based on Wigner distributions

The ray-tracing method we propose is based on the properties of Wigner distributions associated with optical fields, which are defined on a scaled phase-space as explained in Parts I [1] and II [2]. In this section, we consider that the transfer from one spherical cap to another is a real-order transfer (see Part I). Complex-order transfers are dealt with in Sect. 6. To make this part as autonomous as possible, we recall the following.

Consider a light ray propagating from a spherical cap  $\mathcal{A}_1$  (curvature radius  $R_1$ ) to a spherical cap  $\mathcal{A}_2$  (curvature radius  $R_2$ ) at a distance  $D$  (from vertex to vertex). Coordinates are  $x, y$  on  $\mathcal{A}_1$ , and  $x', y'$  on  $\mathcal{A}_2$ . We define

$$J = \frac{(R_1 - D)(D + R_2)}{D(D - R_1 + R_2)}, \quad (7)$$

and assume  $J > 0$ , so that the field transfer by diffraction from  $\mathcal{A}_1$  to  $\mathcal{A}_2$  is a real-order transfer (see Part I [1]): it can then be expressed by a fractional Fourier transformation, whose order  $\alpha$  is defined by  $\alpha D \geq 0$ ,  $-\pi < \alpha < \pi$ , and

$$\cot^2 \alpha = \frac{(R_1 - D)(D + R_2)}{D(D - R_1 + R_2)}. \quad (8)$$

We define the sign of  $\cot \alpha$  by introducing the auxiliary parameter  $\varepsilon_1$  such that

$$\varepsilon_1 = \frac{D}{R_1 - D} \cot \alpha, \quad \varepsilon_1 R_1 > 0. \quad (9)$$

We also introduce

$$\varepsilon_2 = \frac{D}{D + R_2} \cot \alpha, \quad (10)$$

and we proved (Part I):  $\varepsilon_2 R_2 > 0$ .

The ray on  $\mathcal{A}_1$  is  $(\mathbf{r}, \mathbf{\Phi})$ , and corresponding scaled coordinates are

$$\boldsymbol{\rho} = (\rho_x, \rho_y) = \frac{\mathbf{r}}{\sqrt{\lambda \varepsilon_1 R_1}} = \frac{1}{\sqrt{\lambda \varepsilon_1 R_1}}(x, y), \quad (11)$$

$$\boldsymbol{\phi} = (\phi_x, \phi_y) = \sqrt{\frac{\varepsilon_1 R_1}{\lambda}} \mathbf{\Phi} = \sqrt{\frac{\varepsilon_1 R_1}{\lambda}} (\cos \theta_\xi, \cos \theta_\eta). \quad (12)$$

The ray on  $\mathcal{A}_2$  is  $(\mathbf{r}', \mathbf{\Phi}')$ , and scaled coordinates are

$$\boldsymbol{\rho}' = (\rho'_x, \rho'_y) = \frac{\mathbf{r}'}{\sqrt{\lambda \varepsilon_2 R_2}}, \quad (13)$$

$$\boldsymbol{\phi}' = (\phi'_x, \phi'_y) = \sqrt{\frac{\varepsilon_2 R_2}{\lambda}} \mathbf{\Phi}'. \quad (14)$$

In the first part of the paper, we proved:

- In the scaled phase-space, the ray on  $\mathcal{A}_1$  is represented by  $(\boldsymbol{\rho}, \boldsymbol{\phi})$  and the ray on  $\mathcal{A}_2$  by  $(\boldsymbol{\rho}', \boldsymbol{\phi}')$ .
- $(\boldsymbol{\rho}', \boldsymbol{\phi}')$  is deduced from  $(\boldsymbol{\rho}, \boldsymbol{\phi})$  in the rotation whose matrix expression takes the form

$$\begin{pmatrix} \rho'_x \\ \phi'_x \\ \rho'_y \\ \phi'_y \end{pmatrix} = \begin{pmatrix} \cos \alpha & \sin \alpha & 0 & 0 \\ -\sin \alpha & \cos \alpha & 0 & 0 \\ 0 & 0 & \cos \alpha & \sin \alpha \\ 0 & 0 & -\sin \alpha & \cos \alpha \end{pmatrix} \begin{pmatrix} \rho_x \\ \phi_x \\ \rho_y \\ \phi_y \end{pmatrix}. \quad (15)$$

The previous  $4 \times 4$  matrix can be split into two  $2 \times 2$  matrices, operating on two disjoint 2-dimensional subspaces of the phase scaled-space, that is,

$$\begin{pmatrix} \rho'_x \\ \phi'_x \end{pmatrix} = \begin{pmatrix} \cos \alpha & \sin \alpha \\ -\sin \alpha & \cos \alpha \end{pmatrix} \begin{pmatrix} \rho_x \\ \phi_x \end{pmatrix}. \quad (16)$$

and

$$\begin{pmatrix} \rho'_y \\ \phi'_y \end{pmatrix} = \begin{pmatrix} \cos \alpha & \sin \alpha \\ -\sin \alpha & \cos \alpha \end{pmatrix} \begin{pmatrix} \rho_y \\ \phi_y \end{pmatrix}. \quad (17)$$

The ray tracing process is as follows:

1. Given  $\mathcal{A}_1$  and  $\mathcal{A}_2$ , calculate  $J$  (assumed to be positive),  $\alpha$ ,  $\varepsilon_1$  and  $\varepsilon_2$ .
2. Start with a ray  $(\mathbf{r}, \mathbf{\Phi}) = (x, y, \cos \theta_\xi, \cos \theta_\eta)$ .
3. Use Eqs. (11) and (12) to calculate  $\boldsymbol{\rho} = (\rho_x, \rho_y)$  and  $\boldsymbol{\phi} = (\phi_x, \phi_y)$ .
4. Calculate  $(\boldsymbol{\rho}', \boldsymbol{\phi}')$  by applying a rotation of angle  $-\alpha$  to  $(\boldsymbol{\rho}, \boldsymbol{\phi})$ . In practice this is obtained by applying Eqs. (16) and (17).
5. Use Eqs. (13) and (14) to compute  $(\mathbf{r}', \mathbf{\Phi}')$  from  $(\boldsymbol{\rho}', \boldsymbol{\phi}')$ .

### 3 Reentrant rays in stable resonators

#### 3.1 Transfer from one mirror to the other

We consider an optical resonator made up of two spherical mirrors  $\mathcal{M}_1$  and  $\mathcal{M}_2$ . We associate two curvature radii with each mirror: the object radius of  $\mathcal{M}_1$  is  $R_1$  and makes sense before light reflection takes place, that is, when  $\mathcal{M}_1$  is considered as a receiver; the image radius of  $\mathcal{M}_1$  is  $R'_1$  and makes sense after light reflection takes place, that is, when  $\mathcal{M}_1$  is considered as an emitter; these radii are such that  $R'_1 = -R_1$ . The same is done for mirror  $\mathcal{M}_2$  with  $R_2$  and  $R'_2$ .

When expressing diffraction from  $\mathcal{M}_1$  to  $\mathcal{M}_2$ , the algebraic measure to be taken into account is  $D = \overline{\Omega_1 \Omega_2}$  ( $\Omega_1$  is the vertex of  $\mathcal{M}_1$ ;  $\Omega_2$  the vertex of  $\mathcal{M}_2$ ). For diffraction from  $\mathcal{M}_2$  to  $\mathcal{M}_1$ , the algebraic measure to be taken into account is  $D' = \overline{\Omega_2 \Omega_1}$ . Since positive algebraic measure are in the sense of light propagation, which is changed after reflection, we have  $D = D' = L$ , where  $L$  is the ‘‘length’’ of the resonator (see Part I). (In general  $L > 0$ , but some virtual resonators may correspond to  $L < 0$ .)

According to Eq. (7), the parameter  $J$  corresponding to the field transfer from  $\mathcal{M}_1$  to  $\mathcal{M}_2$  is

$$J = \frac{(R'_1 - L)(L + R_2)}{L(L - R'_1 + R_2)}, \quad (18)$$

since  $\mathcal{M}_1$  is considered to be the emitter and  $\mathcal{M}_2$  the receiver. On the other hand, if we regard  $\mathcal{M}_2$  as the emitter and  $\mathcal{M}_1$  as the receiver, the parameter  $J'$  corresponding to the field transfer from  $\mathcal{M}_2$  to  $\mathcal{M}_1$  is

$$J' = \frac{(R'_2 - L)(L + R_1)}{L(L - R'_2 + R_1)}. \quad (19)$$

Since  $R'_1 = -R_1$  and  $R'_2 = -R_2$ , we have  $J' = J$ .

#### 3.2 Stability condition

The following four propositions are equivalent for a resonator to be stable [4, 5]:

1.  $J = J' > 0$ .
2.  $0 \leq \left(1 - \frac{L}{R'_1}\right) \left(1 + \frac{L}{R_2}\right) = \left(1 + \frac{L}{R_1}\right) \left(1 - \frac{L}{R'_2}\right) \leq 1$ .
3. The field transfer from  $\mathcal{M}_1$  to  $\mathcal{M}_2$  is a real-order transfer: the order of the fractional Fourier transformation associated with the field transfer is a real number. (This is equivalent to: the field transfer from  $\mathcal{M}_2$  to  $\mathcal{M}_1$  is a real-order transfer.)
4. Let  $\Omega_1$  and  $C_1$  be respectively the vertex and center of  $\mathcal{M}_1$ ; and  $\Omega_2$  and  $C_2$  be those of  $\mathcal{M}_2$ . The resonator is stable if, and only if, points  $\Omega_1$ ,  $\Omega_2$ ,  $C_1$  and  $C_2$  are arranged on the optical axis in such a way that their indices are ordered according to 1212 or 2121.

#### 3.3 Fractional orders

We assume  $J = J' > 0$ , and we now prove that the fractional orders  $\alpha$  and  $\alpha'$  associated with the respective field transfers from  $\mathcal{M}_1$  to  $\mathcal{M}_2$  and from  $\mathcal{M}_2$  to  $\mathcal{M}_1$  are equal.

The order  $\alpha$  of the fractional Fourier transformation associated with the field transfer from  $\mathcal{M}_1$  to  $\mathcal{M}_2$  is defined by  $\cot^2 \alpha = J$ ,  $\alpha L > 0$ ,  $-\pi < \alpha < \pi$ ; and the order  $\alpha'$  associated with the field transfer from  $\mathcal{M}_2$  to  $\mathcal{M}_1$  by  $\cot^2 \alpha' = J'$ ,  $\alpha' L > 0$ ,  $-\pi < \alpha' < \pi$ . Since  $J = J'$  we conclude  $\cot^2 \alpha' = \cot^2 \alpha$ . The sign of  $\cot \alpha$  is defined according to

$$\varepsilon_1 = \frac{L}{R'_1 - L} \cot \alpha, \quad \varepsilon_1 R'_1 > 0, \quad (20)$$



and is such that (see Appendix A, Part I)

$$\varepsilon_2 = \frac{L}{R_2 + L} \cot \alpha, \quad \varepsilon_2 R_2 > 0. \quad (21)$$

Since  $R'_2 = -R_2$ , Eq. (21) is also

$$\varepsilon_2 = -\frac{L}{R'_2 - L} \cot \alpha, \quad \varepsilon_2 R'_2 < 0. \quad (22)$$

Equivalently, for the transfer from  $\mathcal{M}_2$  to  $\mathcal{M}_1$ , we defined  $\varepsilon'_1$  by

$$\varepsilon'_1 = \frac{L}{R'_2 - L} \cot \alpha', \quad \varepsilon'_1 R'_2 > 0. \quad (23)$$

From  $\varepsilon_2 R'_2 < 0$  and  $\varepsilon'_1 R'_2 > 0$  we conclude that the sign of  $\varepsilon'_1$  is opposite to the sign of  $\varepsilon_2$ , and then, by comparing Eq. (23) with Eq. (22), that  $\cot \alpha$  and  $\cot \alpha'$  have the same sign. Finally we obtain  $\alpha' = \alpha$ .

*Remark.* The order  $\alpha$  can also be defined by

$$\cos^2 \alpha = \left(1 - \frac{L}{R'_1}\right) \left(1 + \frac{L}{R_2}\right) = \left(1 + \frac{L}{R_1}\right) \left(1 - \frac{L}{R'_2}\right). \quad (24)$$

and the additional condition

$$\frac{LR'_1}{R'_1 - L} \cot \alpha > 0, \quad (25)$$

according to Eq. (20)

### 3.4 Round trip

In the first part of the paper, we have shown that, on the one hand, scaled variables on  $\mathcal{M}_1$  are the same both for the transfer from  $\mathcal{M}_1$  to  $\mathcal{M}_2$  and for the transfer from  $\mathcal{M}_2$  to  $\mathcal{M}_1$ ; and on the other hand, that scaled variables on  $\mathcal{M}_2$  are the same for both transfers. Consequently the composition of the corresponding fractional-order Fourier transformations makes sense in representing a round trip from one mirror, including reflection on the other mirror.

### 3.5 Reentrant rays (stable resonators)

A light ray is reentrant if it merges with itself after a finite number of reflections. A ray that propagates along the optical axis is trivially reentrant, whether the resonator is stable or unstable. (Such a ray is perpendicular to both mirrors at their vertices.) In the following, considered reentrant rays are assumed to be non-trivially reentrant rays. In the scaled phase-space, since every transfer from one mirror to the other is expressed by a rotation of angle  $-\alpha$ , if for a given integer  $n$  ( $n > 1$ ) we have  $n\alpha = \pi$ , then every ray is reentrant after  $2n$  reflections. A precise statement is as follows.

**Proposition 3.5.** *Let  $\alpha$  ( $\alpha \neq 0$ ) be the order of the fractional Fourier transformation associated with the field transfer from one mirror to the other mirror of a resonator. Assume  $\alpha$  be such that  $q|\alpha| = m\pi$  where  $q$  and  $m$  are relatively prime integers, and  $q > m > 0$ . Every ray propagating in the resonator is then a reentrant ray, after  $2q$  reflections. Moreover  $2q$  is the least number of reflections for a ray to be reentrant.*

We provide a proof for  $\alpha > 0$  (the adaptation to  $\alpha < 0$  is straightforward). We denote  $\mathbf{p}_1 = (\boldsymbol{\rho}_1, \boldsymbol{\phi}_1) = (\rho_{1x}, \rho_{1y}, \phi_{1x}, \phi_{1y})$  the point  $\mathbf{p}_1$  that represents a ray emerging from mirror  $\mathcal{M}_1$ , in the scaled phase-space. After  $n$  reflections  $\mathbf{p}_1$  becomes  $\mathbf{p}_{n+1}$  that is deduced from  $\mathbf{p}_1$  in the rotation of angle  $-n\alpha$  (which reduces to two rotations of angle  $-\alpha$  in the  $\rho_x$ - $\phi_x$  and  $\rho_y$ - $\phi_y$

subspaces). For the corresponding ray to be reentrant, points  $\mathbf{p}_1$  and  $\mathbf{p}_{n+1}$  should be related to the same mirror ( $\mathcal{M}_1$  or  $\mathcal{M}_2$ ), so that  $n$  has to be an even number. If  $n = 2q$ , we obtain  $n\alpha = 2q\alpha = 2m\pi$  and  $\mathbf{p}_{n+1} = \mathbf{p}_{2q+1} \equiv \mathbf{p}_1$ , and the corresponding ray is reentrant.

Assuming  $\alpha$  positive, we have  $0 < \alpha < \pi$ , and the condition  $q\alpha = m\pi$  can hold only if  $q > m$ . Moreover, since  $q$  and  $m$  are relatively prime,  $m/q$  is a rational number written in its irreducible form, that is, if  $m'/q' = m/q$ , then  $m \leq m'$  and  $q \leq q'$ . Then  $2q$  is the least number of reflections. The proof is complete.  $\square$

The next theorem is a straightforward consequence of Proposition 3.5.

**Theorem.** *Consider a stable resonator. If there exists a ray (non-trivially) reentrant after  $2q'$  reflections ( $q' > 1$ ), then every ray is reentrant after  $2q'$  reflections.*

A proof is as follows. Let  $\alpha$  be the fractional order associated with the resonator; we assume  $0 < \alpha < \pi$  (negative  $\alpha$  is held in a similar way). The representative points, in the subspace  $\rho_x\text{-}\phi_x$ , of the reentrant ray and its reflected rays are on a circle, and  $(\rho_{(j+1)x}, \phi_{(j+1)x})$  is deduced from  $(\rho_{jx}, \phi_{jx})$  in the rotation of angle  $-\alpha$ . Since the considered ray is reentrant after  $2q'$  reflections, we have  $(\rho_{(2q'+1)x}, \phi_{(2q'+1)x}) = (\rho_{1x}, \phi_{1x})$ ; there is then an integer  $m'$  ( $m' > 0$ ) such that  $2q'\alpha = 2m'\pi$ , and  $q' > m'$ , because  $\alpha < \pi$ . Since  $q'/m' = q/m$ , where  $q$  and  $m$  are relatively prime ( $q/m$  is the irreducible form of  $q'/m'$ ), and since  $0 < m < q$ , by Proposition 3.5 we conclude that every ray is reentrant after  $2q$  reflections. Since  $q'$  is a multiple of  $q$ , every ray is also reentrant after  $2q'$  reflections.  $\square$

*Remark.* The  $x$ -component of vector  $\boldsymbol{\rho}_1$  is denoted by  $\rho_{1x}$ , its  $y$ -component by  $\rho_{1y}$ ;  $\phi_{1x}$  and  $\phi_{1y}$  respectively denote the  $x$  and  $y$ -components of vector  $\boldsymbol{\phi}_1$ . Thus  $\rho_{jx}$  denotes the  $x$ -component of  $\boldsymbol{\rho}_j$  and  $\rho_{(2n)x}$  that of  $\boldsymbol{\rho}_{2n}$ , etc.

### 3.6 Interpreting diagrams

In the following, we provide mainly two kinds of diagrams showing reentrant rays in a given resonator. We consider  $x$ - $z$  sections of the resonator and ray representations in the  $\rho_x\text{-}\phi_x$  subspace of the scaled phase-space. The same can be done in the  $\rho_y\text{-}\phi_y$  subspace and it is necessary to use both representations for dealing with skew rays (see Sect. 5).

Figure 7 illustrates how diagrams have to be interpreted (a four-reentrant meridional ray is taken as an example). The main points are as follows.

- Every ray is given a number  $j$ .
- In the physical space, ray  $j$  is issued from point  $M_j$ , which may lie on  $\mathcal{M}_1$  or on  $\mathcal{M}_2$  (Fig. 7). It is considered after reflection on a mirror. We arrange for  $M_{2j+1}$  to belong to  $\mathcal{M}_1$  and  $M_{2j}$  to  $\mathcal{M}_2$ .
- Ray  $j$  is defined by the coordinate  $x_j$  of point  $M_j$ , at which the ray is reflected, and by the angle  $\theta_{nj}$  it makes with the normal to the mirror at  $M_j$ .
- Reflection angles ( $\theta_{nj}$ ) are taken from the normal to the mirror toward the ray. Positive sense for angles related to each mirror are indicated by circles with arrows, see top of Fig. 7 (left). For example in Fig. 7, we have  $\theta_{n1} < 0$ , since  $\theta_{n1}$  is related to  $\mathcal{M}_1$ ; and  $\theta_{n2} < 0$ , since it is related to  $\mathcal{M}_2$ .
- In the scaled phase-space, ray  $j$  is represented by the point (also denoted  $j$ ) of coordinates  $(\rho_{jx}, \phi_{jx})$ , which are related to the mirror from which the ray is issued (that is, after reflection on the mirror).
- All points  $j$  belong to a same circle, as explained in the first part of the paper [1]. The circle radius is given by the initial-ray parameters.
- For example, in Fig. 7, we have  $x_1 > 0$  and  $x_2 < 0$ , and thus  $\rho_{1x} > 0$  and  $\rho_{2x} < 0$ .

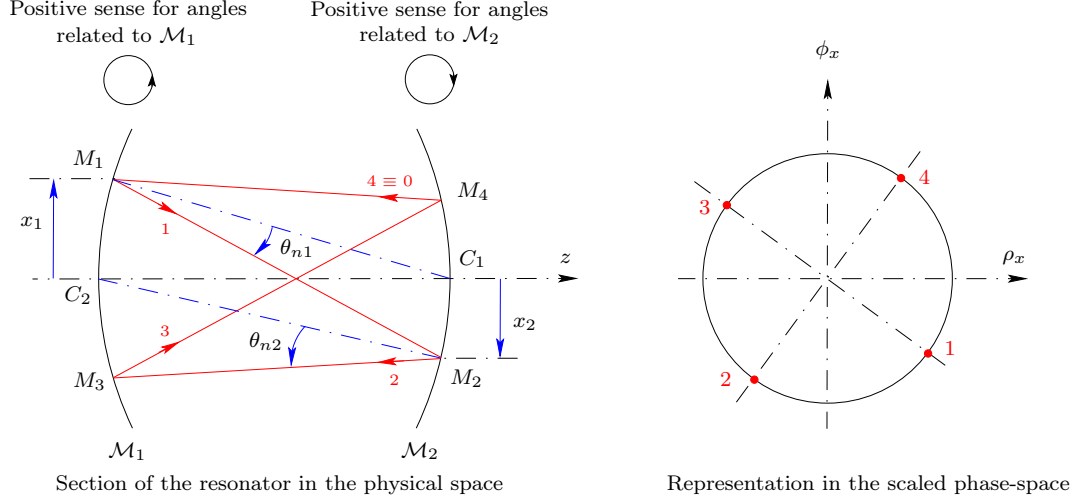


Figure 7: Interpretation of diagrams. Left: section of the resonator in the  $x$ - $z$  plane. Points  $C_1$  and  $C_2$  are the respective curvature centers of  $\mathcal{M}_1$  and  $\mathcal{M}_2$ . On the top, circles with arrows indicate the positive senses for angles, with respect to mirrors; in the above diagram, angles  $\theta_{n1}$  and  $\theta_{n2}$  are both negative. Right: ray representation in the scaled phase-space (in fact in a 2-dimensional subspace). Ray 1, issued from  $M_1$ , has coordinates  $\rho_{1x}$  and  $\phi_{1x}$  in the scaled phase-space and is defined by  $x_1$  and  $\theta_{n1}$  in the physical space. Ray 2, issued from  $M_2$  has coordinates  $\rho_{2x}$  and  $\phi_{2x}$  in the scaled phase-space and is defined by  $x_2$  and  $\theta_{n2}$  in the physical space. Points  $2j + 1$  represent rays after reflections on  $\mathcal{M}_1$ ; points  $2j$  after reflections on  $\mathcal{M}_2$ .

## 4 Tracing reentrant meridional rays in stable resonators

### 4.1 Examples

To illustrate the correspondence between rays in a resonator and their representations in the scaled phase-space we first provide some examples of reentrant meridional rays that can be dealt with simple methods of paraxial geometrical optics. A ray  $j$  is defined by the point  $M_j$  where it intercepts a mirror and the point  $A_j$  where it intercepts the optical axis. The sequence  $(A_j)$  ( $j = 1, 2, 3, \dots$ ) is obtained from paraxial imaging through a spherical mirror (for example by applying Newton's conjugation formula):  $A_{2j}$  is the paraxial image of  $A_{2j-1}$  through  $\mathcal{M}_2$ ; and  $A_{2j+1}$  the image of  $A_{2j}$  through  $\mathcal{M}_1$  (see Fig. 12 for examples). The chosen examples are simple in the meaning that distances from points  $A_j$  to the mirror foci are integer multiples or simple fractions of  $L$  ( $2L, L/2, 2L/3$ , etc.) so that one can work out Newton's formula in one's head.

The following figures show meridional sections of resonators and meridional rays that are obtained according to the above mentioned method. Figures also show ray representations in the scaled phase-space, which are deduced from the previous results (obtained in the physical space).

#### 4.1.1 Two reflections: $q = 1$ and $\alpha = \pi$

Since in the general theory we have  $-\pi < \alpha < \pi$  (see Sect. 2.5 and also Part I), we remark first that  $\alpha = \pi$ , which means that  $\cot \alpha$  is infinite, does not enter in the previous theoretical framework. Nevertheless,  $\alpha = \pi$  can be obtained for example if  $2R'_1 = L = -2R_2$ ; mirrors  $\mathcal{M}_1$  and  $\mathcal{M}_2$  are then concentric (Fig. 8). In fact such a resonator is at the boundary between stable and unstable resonators, since vertices and curvature centers are arranged according to  $(\Omega_1, C_1 = C_2, \Omega_2)$ : if  $\mathcal{M}_1$  is slightly moved to the left, the arrangement becomes  $(\Omega_1, C_1, C_2, \Omega_2)$ , and the resonator is unstable; if  $\mathcal{M}_1$  is slightly moved to the right, the arrangement becomes  $(\Omega_1, C_2, C_1, \Omega_2)$  and the resonator is stable.

Every ray perpendicular to  $\mathcal{M}_1$  passes by the mirror center ( $C_1 = C_2$ ) and is incident perpen-

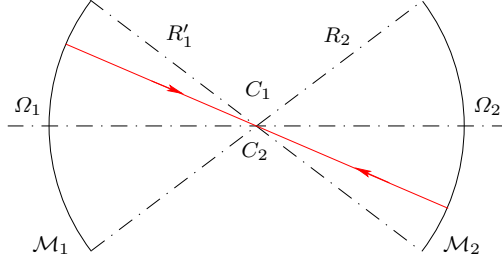


Figure 8: Meridional section of a resonator made up of two concentric mirrors ( $2R'_1 = L = -2R_2$ ). Reentrant ray after 2 reflections.

dicular to  $\mathcal{M}_2$ : it is a reentrant ray, as shown in Fig. 8. Note that rays that are not orthogonal to a mirror—and do not pass by the mirror center—are not reentrant: Proposition 3.5 does not apply for  $q = 1$ .

#### 4.1.2 Four reflections: $q = 2$ and $\alpha = \pi/2$

The value  $\alpha = \pi/2$  can be obtained for example with a symmetric confocal resonator for which  $R'_1 = L = -R_2$  (Fig. 9). Each mirror is centered on the other mirror ( $\Omega_1 = C_2$  and  $\Omega_2 = C_1$ ); the mirror foci are merged with the midpoint between the vertices. The resonator is at the boundary between stable and unstable resonators, because the arrangement of vertices and curvature centers of mirrors is  $(\Omega_1 = C_2, C_1 = \Omega_2)$ : slightly moving  $\mathcal{M}_1$  to the left (or  $\mathcal{M}_2$  to the right) makes the arrangement become  $(\Omega_1, C_2, C_1, \Omega_2)$  and the resonator becomes stable; slightly moving both  $\Omega_1$  and  $\Omega_2$  to the left (without moving  $C_1$  and  $C_2$ ) makes the resonator become unstable.

Since we consider meridional rays, the analysis in the scaled phase-space can be done according to coordinates  $\rho_x, \phi_x$  only, that is, setting  $(\rho_y, \phi_y) = (0, 0)$  for all rays. Figure 9 illustrates three examples of reentrant meridional rays, after 4 reflections. The analysis is as follows.

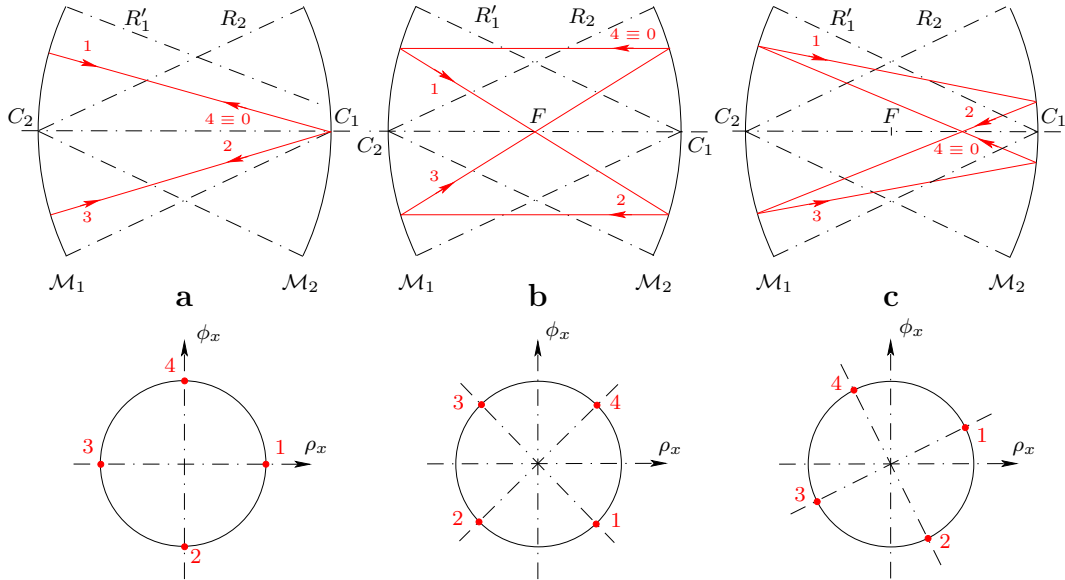


Figure 9: Three examples of reentrant meridional rays after 4 reflections ( $\alpha = \pi/2$ ). Mirrors  $\mathcal{M}_1$  and  $\mathcal{M}_2$  are symmetric confocal. Top: meridional sections of the resonator and meridional reentrant rays. Bottom: ray representations in the scaled phase-space.

1. Fig. 9–a. Ray 1 is orthogonal to  $\mathcal{M}_1$  and passes by  $C_1$  the center of  $\mathcal{M}_1$ , which is also the vertex of  $\mathcal{M}_2$ . Then ray 2 is symmetrical to ray 1 with respect to the optical axis and is incident orthogonal to  $\mathcal{M}_1$ ; rays 2 and 3 are supported by a same straight line. In the scaled phase-space, ray 1 is represented by point 1, whose coordinates are  $\rho_{1x}$  and  $\phi_{1x} = 0$  (because ray 1 is orthogonal to  $\mathcal{M}_1$ ). Coordinate  $\rho_{1x}$  is given by Eq. (11),  $x_1$  being the  $x$ -coordinate (in the physical space) of  $M_1$ , the point where the initial ray intercepts  $\mathcal{M}_1$ . The radius of the circle on which ray representative points are located is equal to  $\rho_{1x}$ . In the scaled phase-subspace, point 2 is deduced from point 1 in the rotation of angle  $-\pi/2$ , and is such that  $(\rho_{2x}, \phi_{2x}) = (0, -\rho_{1x})$ .
2. Fig. 9–b. Mirrors  $\mathcal{M}_1$  and  $\mathcal{M}_2$  are confocal: their common focus  $F$  is the midpoint of segment  $C_1C_2$ . Ray 1 passes by  $F$  and it is reflected in ray 2, which is parallel to the optical axis. After reflection on  $\mathcal{M}_1$ , ray 2 becomes ray 3, which passes by the focus  $F$  and it is reflected in ray 4, which is parallel to the optical axis. Since  $x_1 = x_4$  (in the physical space), points 1 and 4 are symmetrical with respect to the  $\rho_x$  axis, in the scaled phase-subspace. And since point 1 is deduced from point 4 in the rotation of angle  $-\pi/2$ , point 1 is at  $-45^\circ$  on the circle.
3. Fig. 9–c. Let  $f'$  denote the image focal length of mirror  $\mathcal{M}_2$ . Ray 1 intercepts the optical axis at point  $A_1$ , at a distance  $|2f'|$  from the focus (that is  $C_1A_1 = \Omega_2A_1 = |2f'|$ ,  $A_1$  is virtual), and the image of  $A_1$  through  $\mathcal{M}_2$  is  $A_2$  such that  $FA_2 = |f'|/2$ :  $A_2$  is the midpoint of segment  $FC$ . Since both mirrors share a common focus, the point  $A_1$  is the image of  $A_2$  through  $\mathcal{M}_1$ , so that  $A_3 \equiv A_1$ , and ray 3 (virtually) passes by  $A_1$ . Finally ray 4 passes by  $A_4 \equiv A_2$ , and is reflected in ray 1.

#### 4.1.3 Six reflections: $q = 3$ and $\alpha = \pi/3$

This is obtained for example when  $R'_1 = 2L = -R_2 = R'_2 > 0$  (Fig. 10). The arrangement of vertices and curvature centers is  $(C_2, \Omega_1, \Omega_2, C_1)$  and the resonator is stable. Every ray is reentrant after 6 reflections. Two examples are given in Fig. 10. Comments are as follows.

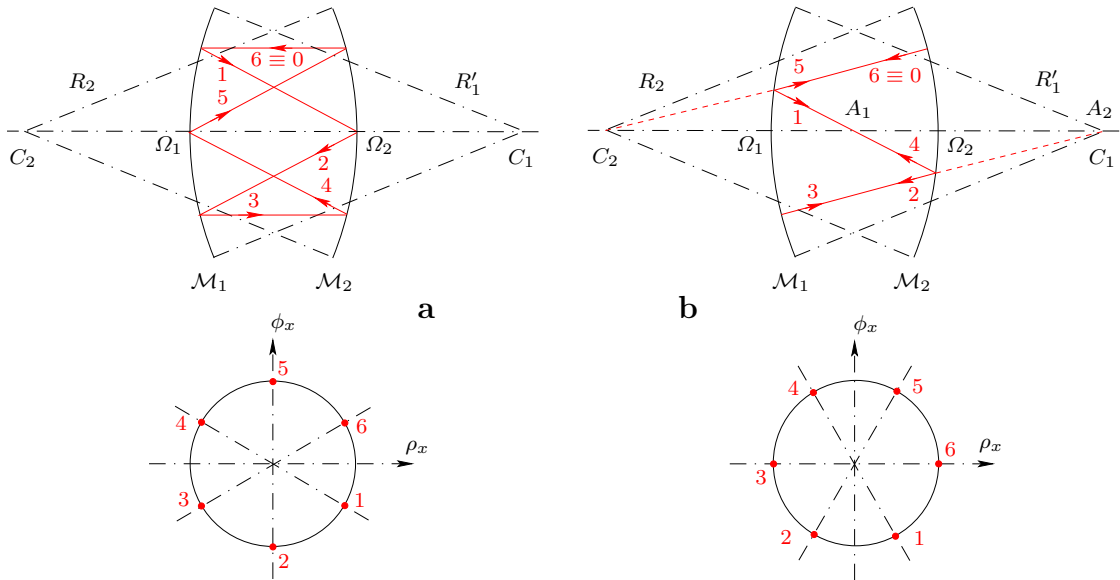


Figure 10: Reentrant meridional rays after 6 reflections:  $R'_1 = 2L = -R_2$  and  $\alpha = \pi/3$ . Right (b): rays 2 and 3 are orthogonal to  $\mathcal{M}_1$ ; rays 5 and 6 are orthogonal to  $\mathcal{M}_2$ .

1. Fig. 10-a. Ray 1 is reflected in ray 2, which is its symmetrical with respect to the optical axis. Since  $\Omega_1$  is the midpoint of  $C_2\Omega_2$ , it is also the focus of  $\mathcal{M}_2$ ; then ray 3 is parallel to the optical axis, and ray 4 converges at  $\Omega_1$ , the focus of  $\mathcal{M}_2$ . But  $\Omega_1$  is also the vertex of  $\mathcal{M}_1$  and ray 5 is then symmetrical to ray 4 with respect to the optical axis. Since  $\Omega_1$  is the focus of  $\mathcal{M}_2$ , ray 6 is parallel to the optical axis.
2. Fig. 10-b. Ray 1 passes at point  $A_1$ , which is the midpoint of  $\Omega_1\Omega_2$ . Since  $|f'| = \Omega_1\Omega_2$  is the focal length of  $\mathcal{M}_1$  and  $\Omega_2$  its focus, ray 2, which is the image of ray 1 through  $\mathcal{M}_1$ , passes through the image  $A_2$  of  $A_1$  through  $\mathcal{M}_2$ . Newton's conjugation formula shows that  $A_2 = C_1$ ; then ray 2 is incident orthogonal to  $\mathcal{M}_1$  and is reflected in ray 3, orthogonal to  $\mathcal{M}_1$ . Rays 4, 5 and 6 are analyzed in the same way.

#### 4.1.4 Twelve reflections: $q = 6$ and $\alpha = \pi/6$

This is obtained for  $R'_1 = 2L = R_2 = -R'_2 > 0$  (Fig. 11). The arrangement of vertices and curvature centers is  $(\Omega_1, \Omega_2, C_1, C_2)$  and the resonator is stable.

- In Fig. 11, the vertex of  $\mathcal{M}_2$ , i.e.  $\Omega_2$ , is also the focus of  $\mathcal{M}_1$ , and the center of  $\mathcal{M}_1$ , i.e.  $C_1$ , is also the focus of  $\mathcal{M}_2$ . Ray 1, orthogonal to  $\mathcal{M}_1$ , (virtually) passes by  $C_1$ , which is also the focus of  $\mathcal{M}_2$ , and is then reflected in ray 2, which is parallel to the optical axis. Ray 2 is reflected in ray 3, which passes by the focus of  $\mathcal{M}_1$ , that is, by  $\Omega_2$ . Ray 4 is symmetrical to ray 3 with respect to the optical axis, and since it passes by  $\Omega_2$ , which is also the focus of  $\mathcal{M}_1$ , it is reflected in ray 5, which is parallel to the optical axis. Its image through  $\mathcal{M}_2$  is ray 6, which passes by the focus of  $\mathcal{M}_2$ , that is by  $C_1$ ; this means that ray 6 is incident perpendicular to  $\mathcal{M}_1$ , so that ray 6 and ray 7 have the same straight line as support, and this holds true for rays 8 and 5, and for rays 9 and 4. Rays 10, 11 and 12 are analyzed in a similar way.
- Figure 12 provides another example. The image focal lengths of both mirror are  $f' = L$ , so that the focus of  $\mathcal{M}_1$  is  $\Omega_2$  (the vertex of  $\mathcal{M}_2$ ), and the focus of  $\mathcal{M}_2$  is  $C_1$  (the curvature center of  $\mathcal{M}_1$ ). Ray 1 is chosen such that  $\overline{\Omega_1 A_1} = -L$ . Then  $\overline{C_1 A_1} = -3L$  and Newton's conjugation formula gives  $\overline{C_1 A_2} = -L/3$ . Then  $A_3$  is the image of  $A_2$  through  $\mathcal{M}_1$ , and we calculate  $\overline{\Omega_2 A_3} = 3L/2$ , etc.

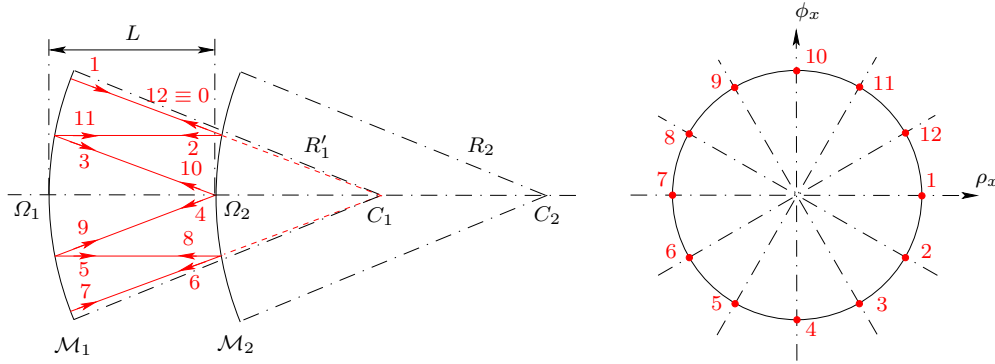


Figure 11: Reentrant meridional rays after 12 reflections:  $R'_1 = 2L = R_2 > 0$ , and  $\alpha = \pi/6$ . Rays 1 and 12, and rays 6 and 7, are orthogonal to  $\mathcal{M}_1$ .

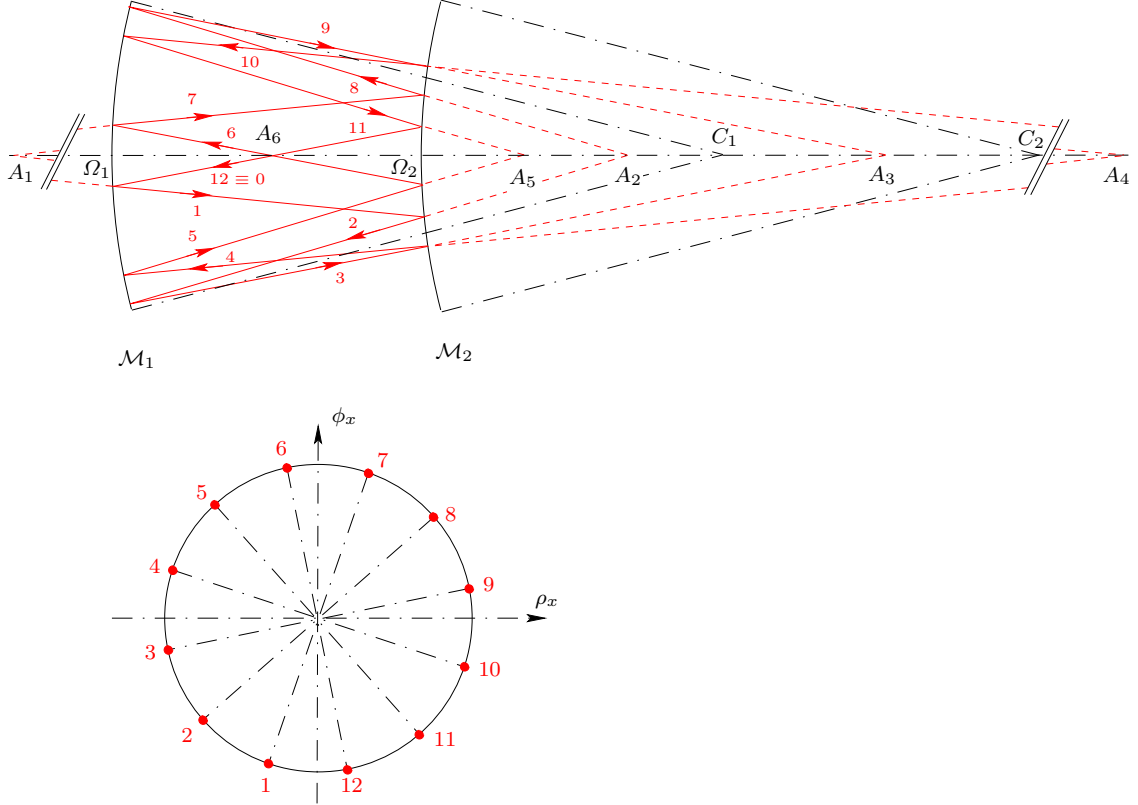


Figure 12: Reentrant meridional rays after 12 reflections:  $R'_1 = 2L = R_2$ , and  $\alpha = \pi/6$ . Top: Ray  $j$  intercepts the optical axis at  $A_j$ . Point  $A_{2j}$  is the paraxial image of  $A_{2j-1}$  through  $\mathcal{M}_2$ ; point  $A_{2j+1}$  is the paraxial image of  $A_{2j}$  through  $\mathcal{M}_1$ . We have  $A_{j+6} \equiv A_j$ .

## 4.2 Application of the proposed method: a numerical example

In a way, the proposed method, described in Sect. 2.5, is opposite to the previous one, described in Sect. 4.1, since ray tracing in meridional sections is now deduced from diagrams in the scaled phase-space and from corresponding numerical values. A ray is defined by two points, which are linked by a rotation in the scaled phase-space, and physical coordinates are deduced from scaled ones.

### 4.2.1 Remark on numerical values

The following numerical calculi have been performed with a Hewlett-Packard HP 35 S scientific calculator, which generally represents numbers with 12 significative decimal digits. We processed numbers by keeping, as far as possible, the full precision of the calculator. Providing results with 6 or 7 significative decimal digits, as generally done in the following, has no physical meaning in geometrical optics (2 or 3 digits accuracy would be more than enough). We proceed this way to allow the reader to check our numerical results.

Angles are expressed in radians or in decimal degrees (for example  $10.25^\circ$ , which is equal to  $10^\circ 15'$ ).

### 4.2.2 Coordinates of a ray

Before developing an explicit example of the proposed method, we recall that a ray is represented in the physical space by  $(\mathbf{r}, \Phi) = (x, y, \cos \theta_\xi, \cos \theta_\eta)$  and in the scaled phase-space by a point

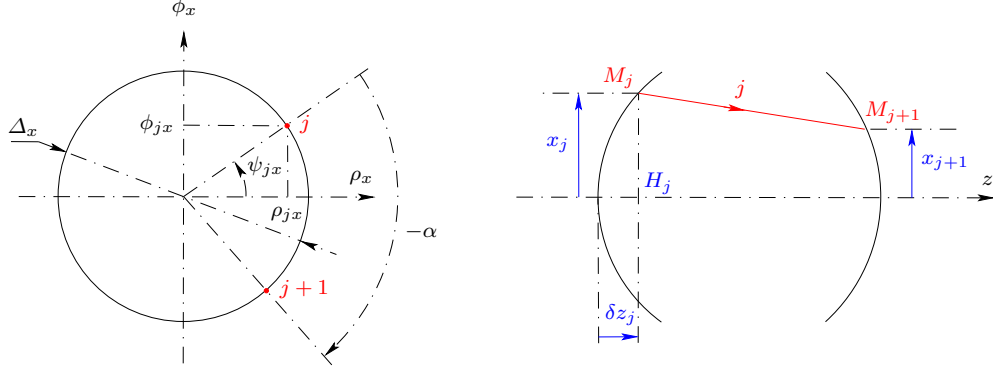


Figure 13: Meridional ray in the  $x$ - $z$  plane. Left: ray  $j$  is represented by point  $j$ , whose coordinates in the scaled phase-space are  $\rho_{jx}$  and  $\phi_{jx}$ . Point  $j+1$  is deduced from point  $j$  in the rotation of angle  $-\alpha$  (see Part I). Representative points of all the reflected rays issued from a given ray lie on a circle whose diameter is denoted  $\Delta_x$ . Given  $\Delta_x$ , the point  $j$  is also defined by the angle  $\psi_{jx}$ . Right: knowing  $x_j$  and  $x_{j+1}$  is enough for tracing ray  $j$  between  $M_j$  and  $M_{j+1}$ . Coordinate  $x_j$  is directly deduced from  $\rho_{jx}$ , so that knowing successive points 1, 2, 3, ... of the diagram on the left leads to ray tracing on the right diagram.

$\mathbf{p} = (\rho_x, \phi_x, \rho_y, \phi_y)$ . A meridional ray propagates in a meridional plane and we shall assume that the considered plane is the  $x$ - $z$  plane. Let  $M$  be a point on a mirror and belonging to the plane  $x$ - $z$ . The normal vector  $\mathbf{e}_n$  to the mirror at point  $M$  is also in the plane  $x$ - $z$ , so that  $\mathbf{e}_n$  is orthogonal to the same plane. Finally, for a meridional ray in the plane  $x$ - $z$ , we have  $y = 0$  and  $\cos \theta_\eta = 0$ : the ray is totally defined, in the meridional plane  $x$ - $z$ , by  $(x, \cos \theta_\xi)$ . Consequently, for the previous meridional ray, we have  $\rho_y = 0$  and  $\phi_y = 0$ , and the ray is represented by the point  $(\rho_x, \phi_x)$  in a two-dimensional subspace of the scaled phase-space. As proved in Part I, all the representative points of successive reflected rays issued from a given initial meridional ray lie on a circle, whose diameter will be denoted by  $\Delta_x$  (Fig. 13).

The ray after  $j$  reflections is called “ray  $j$ ,” and we assume that the first reflection is on mirror  $\mathcal{M}_1$ . Coordinates of ray  $j$  are  $\rho_{jx}$  and  $\phi_{jx}$ . Ray 1 will be given a priori, and

$$\Delta_x = \sqrt{(\rho_{1x})^2 + (\phi_{1x})^2}. \quad (26)$$

Since  $\Delta_x$  is a constant, point  $j$  is also defined by the angle  $\psi_{jx}$ , such that (Fig. 13)

$$\tan \psi_{jx} = \frac{\phi_{jx}}{\rho_{jx}}. \quad (27)$$

We remark that for a meridional ray, given an initial ray, that is, given  $\Delta_x$ , the knowledge of  $\psi_{jx}$  is enough to locate the point  $j$  on the circle and then to determine the corresponding ray in the section  $x$ - $z$  of the resonator.

The complete coordinates of point  $M_j$  are  $x_j$ ,  $y_j = 0$ , and  $\delta z_j = \overline{\Omega_1 N_j}$ , if  $M_j$  is on  $\mathcal{M}_1$ ; and  $\delta z_j = \overline{\Omega_2 N_j}$ , if  $M_j$  is on  $\mathcal{M}_2$ , being  $N_j$  the orthogonal projection of  $M_j$  on the optical axis (see Fig. 13). We have (binomial series)

$$\delta z_{2j+1} = \frac{(x_{2j+1})^2}{2R'_1} + \frac{(x_{2j+1})^4}{8(R'_1)^3} + \dots \quad (28)$$

and

$$\delta z_{2j} = \frac{(x_{2j})^2}{2R_2} + \frac{(x_{2j})^4}{8(R_2)^3} + \dots \quad (29)$$

Finally, we point out that for a meridional ray in the plane  $x$ - $z$ , we have  $\theta_\xi = (\pi/2) - \theta_n$ , where  $\theta_n$  is the angle from the normal to the ray. Then  $\cos \theta_\xi = \sin \theta_n$  and  $|\Phi| = |\sin \theta_n|$ .



### 4.2.3 Defining parameters

We consider the resonator of Fig. 10:  $R'_1 = 2L = -R_2 > 0$ , and  $\alpha = \pi/3$ . For an example of ray tracing, we choose ray 1 as being the meridional ray defined by  $\mathbf{r}_1 = (x_1, 0)$ ,  $x_1 = L/2$ , and  $\Phi_1 = (\sin \theta_{n1}, 0)$ , with  $\theta_{n1} = 10^\circ$ . Since  $R'_1 = 2L$ , we have

$$\varepsilon_1 = \frac{L}{R'_1 - L} \cot \alpha = \cot \frac{\pi}{3} = 0.577350, \quad (30)$$

and, according to Eq. (10), since  $2L = -R_2$ ,

$$\varepsilon_2 = \frac{L}{R_2 + L} \cot \alpha = -\cot \frac{\pi}{3} = -0.577350. \quad (31)$$

Scaled coordinates of ray 1 are

$$\rho_{1x} = \frac{1}{\sqrt{\varepsilon_1}} \frac{x_1}{\sqrt{\lambda R'_1}} = \frac{1}{2\sqrt{2}\sqrt{\varepsilon_1}} \sqrt{\frac{L}{\lambda}}, \quad (32)$$

$$\phi_{1x} = \sqrt{\varepsilon_1} \sqrt{\frac{R'_1}{\lambda}} \sin \theta_{n1} = \sqrt{2}\sqrt{\varepsilon_1} \sqrt{\frac{L}{\lambda}} \sin \theta_{n1}. \quad (33)$$

so that we shall develop calculi taking  $\sqrt{L/\lambda}$  as unit.

All points representing successive reflected rays are on the circle whose diameter is  $\Delta_x$ , with

$$\frac{\Delta_x}{2} = \sqrt{(\rho_{1x})^2 + (\phi_{1x})^2} = \sqrt{\frac{1}{8\varepsilon_1} + 2\varepsilon_1 \sin^2 \theta_{n1}} \sqrt{\frac{L}{\lambda}}. \quad (34)$$

Scaled variables of successive rays on  $\mathcal{M}_1$  are

$$\rho_{(2j+1)x} = \frac{1}{\sqrt{2}\sqrt{\varepsilon_1}} \frac{x_{2j+1}}{\sqrt{\lambda L}}, \quad (35)$$

$$\phi_{(2j+1)x} = \sqrt{2}\sqrt{\varepsilon_1} \sqrt{\frac{L}{\lambda}} \sin \theta_{n(2j+1)}. \quad (36)$$

Since  $-\varepsilon_2 = \varepsilon_1 > 0$  and  $-R_2 = R'_1 > 0$ , scaled variables on  $\mathcal{M}_2$  are

$$\rho_{(2j)x} = \frac{1}{\sqrt{|\varepsilon_2|}} \frac{x_{2j}}{\sqrt{\lambda |R_2|}} = \frac{1}{\sqrt{2}\sqrt{\varepsilon_1}} \frac{x_{2j}}{\sqrt{\lambda L}}, \quad (37)$$

$$\phi_{(2j)x} = \sqrt{|\varepsilon_2|} \sqrt{\frac{|R_2|}{\lambda}} \sin \theta_{n(2j)} = \sqrt{2}\sqrt{\varepsilon_1} \sqrt{\frac{L}{\lambda}} \sin \theta_{n(2j)}. \quad (38)$$

Table 1 summarizes the previous parameters and initial values.

### 4.2.4 Actual ray tracing

Starting with ray 1, the successive reflected rays are defined by their angles  $\psi_{jx}$ , such that

$$\psi_{(j+1)x} = \psi_{jx} - 60^\circ \bmod 360^\circ. \quad (39)$$

Then  $\rho_{jx} = (\Delta_x/2) \cos \psi_{jx}$  and since  $\cos \psi_{jx} \neq 0$ , we use

$$\frac{x_j}{x_1} = \frac{\rho_{jx}}{\rho_{1x}} = \frac{\cos \psi_{jx}}{\cos \psi_{1x}}. \quad (40)$$

Numerical results are given in Table 2 and illustrated in Figs. 14 and 15. In Table 2, parameter  $x_1$  is taken as unit; since  $x_1 = L/2$  we have

$$x_j = \frac{x_j}{x_1} \frac{L}{2}. \quad (41)$$

Parameter	Definition	Numerical value
$\alpha$	$\cot^2 \alpha = J > 0$	$\pi/3$
$\varepsilon_1$	$\frac{L}{R'_1 - L} \cot \alpha = \cot \alpha$	0.577 350
$\varepsilon_2$	$\frac{L}{R_2 + L} \cot \alpha = -\cot \alpha$	-0.577 350
$x_1$		$L/2$
$\theta_{n1}$		$10^\circ$
$\mathbf{r}_1$	$(x_1, 0)$	$(L/2, 0)$
$\Phi_1$	$(\xi_1, \eta_1) = (\sin \theta_{n1}, 0)$	$(0.173\ 648, 0)$
$\rho_{1x}$	$\frac{1}{\sqrt{\varepsilon_1}} \frac{x_1}{\sqrt{2\lambda L}} = \frac{1}{2\sqrt{2}\sqrt{\varepsilon_1}} \sqrt{\frac{L}{\lambda}}$	$0.465\ 302 \sqrt{\frac{L}{\lambda}}$
$\phi_{1x}$	$\sqrt{2}\sqrt{\varepsilon_1} \sqrt{\frac{L}{\lambda}} \sin \theta_{n1}$	$0.186\ 597 \sqrt{\frac{2L}{\lambda}}$
$\Delta_x/2$	$\sqrt{(\rho_{1x})^2 + (\phi_{1x})^2}$	$0.501\ 323 \sqrt{\frac{L}{\lambda}}$
$\psi_{1x}$	$\tan \psi_{1x} = \frac{\phi_{1x}}{\rho_{1x}}$	$21.851\ 935^\circ$

Table 1: Numerical values of parameters and initial data for ray tracing in a stable resonator such that  $R'_1 = 2L = -R_2 > 0$ . The initial ray pierces the mirror at abscissa  $x_1 = L/2 = R'_1/4$ . Some values are expressed as multiples of  $\sqrt{L/\lambda}$ . To make checkings easier, we provide numerical results with a precision higher than physically significant (see Sect. 4.2.1).

$j$	$\psi_{jx}$	$\frac{x_j}{x_1}$	$x_j$
1	$21.851\ 935^\circ$	1	$0.5 L$
2	$-38.148\ 065^\circ$	0.847 296	$0.423\ 648 L$
3	$-98.148\ 065^\circ$	-0.152 704	$-0.076\ 352 L$
4	$-158.148\ 065^\circ$	-1	$-0.500\ 000 L$
5	$141.851\ 935^\circ$	-0.847 296	$-0.423\ 648 L$
6	$81.851\ 935^\circ$	0.152 704	$0.076\ 352 L$

Table 2: Successive abscissae of a ray, reentrant after 6 reflections. Data correspond to Table 1.

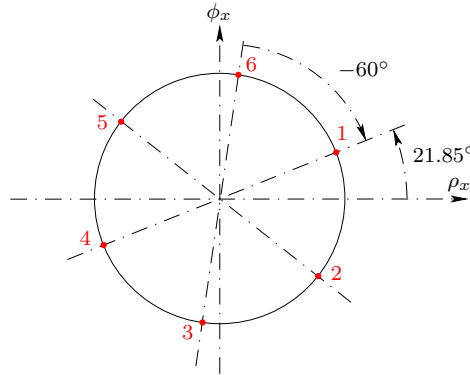


Figure 14: Reentrant meridional rays after 6 reflections:  $R'_1 = 2L = R_2$ , and  $\alpha = \pi/3$ . Data are those of Table 2. The circle radius is equal to  $0.501\ 323 \sqrt{L/\lambda}$ .

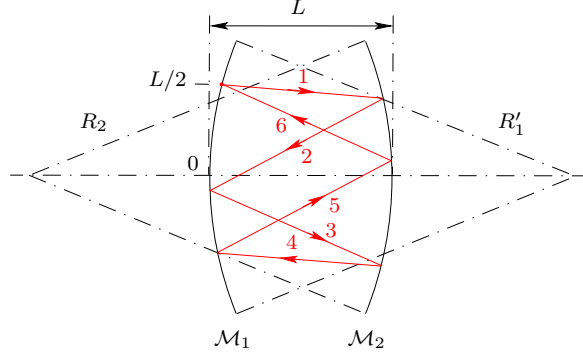


Figure 15: Meridional rays, reentrant after 6 reflections:  $R'_1 = 2L = -R_2 > 0$ , and  $\alpha = \pi/3$ . Ray-tracing is deduced from data of Table 2 and corresponds to Fig. 14.

## 5 Reentrant skew rays in stable resonators

### 5.1 An example

#### 5.1.1 Parameters

Consider the resonator of Sect. 4.1.2, for which  $R'_1 = L = -R_2 > 0$ , and  $\alpha = \pi/2$ . Every ray is reentrant after four reflections.

The transfer from  $\mathcal{M}_1$  to  $\mathcal{M}_2$  is related to parameters  $\varepsilon_1$  and  $\varepsilon_2$  such that

$$\varepsilon_1 = \frac{L}{R'_1 - L} \cot \alpha, \quad \varepsilon_2 = \frac{L}{R_2 + L} \cot \alpha, \quad (42)$$

and which are undetermined for  $\alpha = \pi/2$  and the given curvature radii. According to the definition of  $\varepsilon_1$ , we also have

$$\varepsilon_1^2 = \frac{L(L + R_2)}{(R'_1 - L)(L - R'_1 + R_2)}, \quad (43)$$

so that from  $R'_1 = -R_2$  we obtain  $\varepsilon_1^2 = 1$ , and since  $\varepsilon_1 R'_1 > 0$  and  $R'_1 > 0$ , we conclude  $\varepsilon_1 = 1$ . Similarly,  $\varepsilon_2$  is such that

$$\varepsilon_2^2 = \frac{L(R'_1 - L)}{(R_2 + L)(L - R'_1 + R_2)}, \quad (44)$$

and from  $\varepsilon_2 R_2 > 0$  and  $R_2 < 0$ , we obtain  $\varepsilon_2 = -1$ .

The field transfer from  $\mathcal{M}_2$  is related to the same previous parameters. A point  $\mathbf{r} = (x, y)$  on  $\mathcal{M}_1$  has scaled coordinates

$$\boldsymbol{\rho} = (\rho_x, \rho_y) = \frac{\mathbf{r}}{\sqrt{\lambda \varepsilon_1 R'_1}}, \quad (45)$$

and a point  $\mathbf{r}' = (x', y')$  on  $\mathcal{M}_2$  has scaled coordinates

$$\boldsymbol{\rho}' = (\rho'_x, \rho'_y) = \frac{\mathbf{r}'}{\sqrt{\lambda \varepsilon_2 R_2}}, \quad (46)$$

and since  $\varepsilon_1 R'_1 = \varepsilon_2 R_2$ , we conclude that scaled coordinates are the same on both mirrors, so that taking into account  $\varepsilon_1 = 1$ , we can write, for successive points representing light rays,

$$\boldsymbol{\rho}_j = (\rho_{jx}, \rho_{jy}) = \frac{1}{\sqrt{\lambda R'_1}} (x_j, y_j). \quad (47)$$

Scaled (spatial) angular frequencies are

$$\phi = \sqrt{\frac{\varepsilon_1 R'_1}{\lambda}} (\cos \theta_\xi, \cos \theta_\eta), \quad (48)$$

on  $\mathcal{M}_1$  and

$$\phi' = \sqrt{\frac{\varepsilon_2 R_2}{\lambda}} (\cos \theta'_\xi, \cos \theta'_\eta), \quad (49)$$

on  $\mathcal{M}_2$ . Since  $\varepsilon_1 = 1$  and  $\varepsilon_1 R'_1 = \varepsilon_2 R_2$ , for successive rays we have

$$\phi_j = \sqrt{\frac{R'_1}{\lambda}} (\cos \theta_{\xi j}, \cos \theta_{\eta j}). \quad (50)$$

where  $\theta_{\xi j}$  and  $\theta_{\eta j}$  are the values of  $\theta_\xi$  and  $\theta_\eta$  related to ray  $j$ .

### 5.1.2 Given ray

We choose ray 1 (it is the ray after one reflection on  $\mathcal{M}_1$ ) such that

$$\mathbf{r}_1 = (x_1, y_1) = \left( \frac{L}{3}, 0 \right), \quad (51)$$

$$\Phi_1 = (\xi_1, \eta_1) = (0, \cos \theta_{\eta 1}) = (0, \sin \theta_{n1}), \quad \theta_{n1} = 10^\circ. \quad (52)$$

Since  $R'_1 = L$ , we obtain

$$\boldsymbol{\rho}_1 = (\rho_{1x}, \rho_{1y}) = \frac{1}{3} \sqrt{\frac{R'_1}{\lambda}} (1, 0) = \frac{1}{3} \sqrt{\frac{L}{\lambda}} (1, 0), \quad (53)$$

$$\boldsymbol{\phi}_1 = (\phi_{1x}, \phi_{1y}) = \sqrt{\frac{R'_1}{\lambda}} (0, \sin \theta_{n1}) = \sqrt{\frac{L}{\lambda}} (0, 0.173648). \quad (54)$$

The evolutions of rays in the scaled phase-space are described by using two circles: one lies in the  $\rho_x$ - $\phi_x$  plane and its diameter is  $\Delta_x$ ; the other lies in the  $\rho_y$ - $\phi_y$  plane and its diameter is  $\Delta_y$ . We have

$$\frac{\Delta_x}{2} = \sqrt{(\rho_{1x})^2 + (\phi_{1x})^2} = 0.333333 \sqrt{\frac{L}{\lambda}}, \quad (55)$$

$$\frac{\Delta_y}{2} = \sqrt{(\rho_{1y})^2 + (\phi_{1y})^2} = 0.173648 \sqrt{\frac{L}{\lambda}}. \quad (56)$$

### 5.1.3 Ray tracing

The ray tracing is achieved by using the diagrams of Fig. 16. Figure 17 provides orthographic projections of both the resonator and the reentrant ray, deduced from Fig. 16. Figure 18 provides an oblique projection of the same.

According to Eq. (28) we have

$$\delta z_1 = \delta z_3 \approx \frac{1}{2L} \left( \frac{L}{3} \right)^2 - \frac{1}{8L^3} \left( \frac{L}{3} \right)^4 \approx \frac{L}{18} - \frac{L}{648} \approx 0.057L. \quad (57)$$

We also have

$$\delta z_4 = \delta z_2 \approx \frac{y_2^2}{2R_2} + \frac{y_2^4}{8R_2^3}, \quad (58)$$

where  $y_2 = \rho_{2y} \sqrt{\lambda \varepsilon_2 R_2}$ . Since  $R_2 = -L$  and  $\rho_2 = \Delta_y/2$  we obtain  $y_2 \approx 0.174L$  and

$$\delta z_4 = \delta z_2 \approx -\frac{0.174^2}{2} L - \frac{0.174^4}{8} L \approx -0.015L. \quad (59)$$

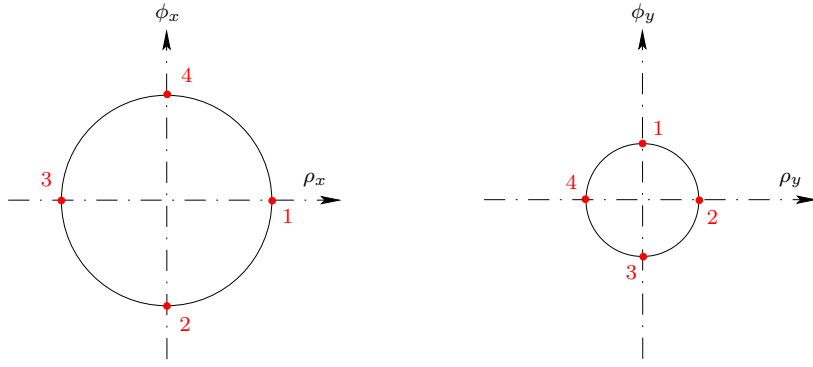


Figure 16: Skew rays reentrant after 4 reflections. Representative points of successive rays in the scaled phase-space. Left: the radius of the circle is  $\sqrt{L/\lambda}/3$ . Right: the circle radius is  $0.173\,648\sqrt{L/\lambda}$ .

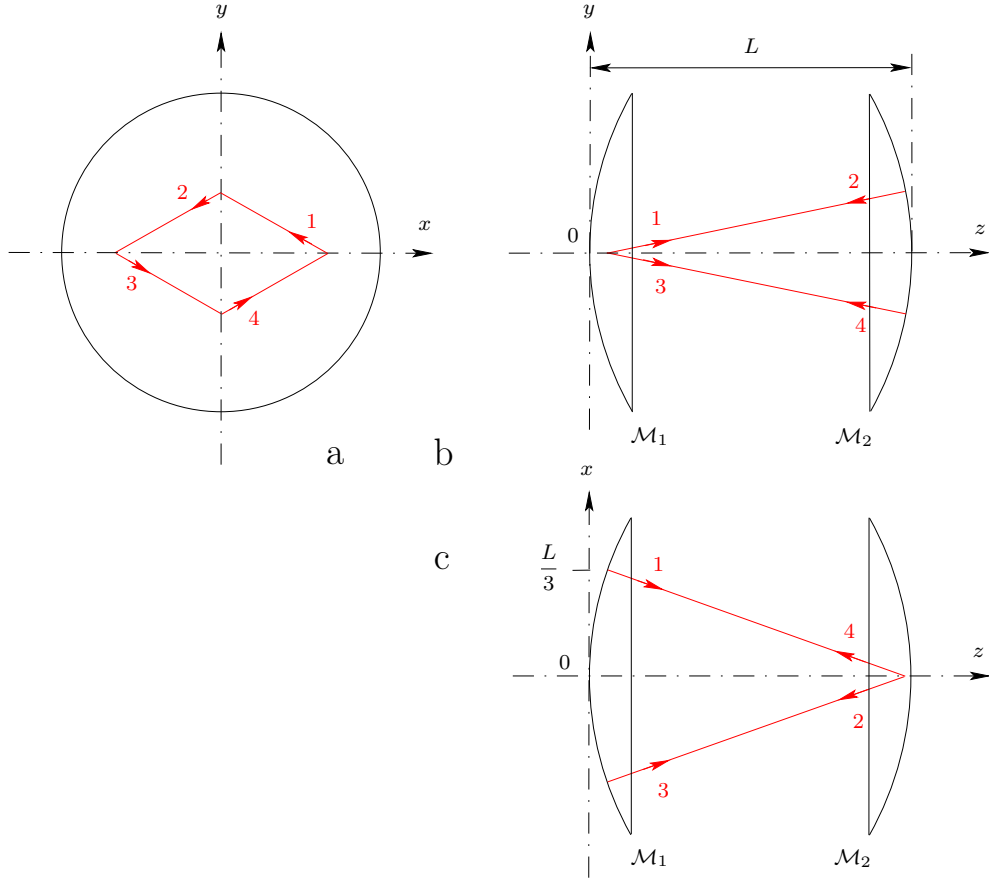


Figure 17: Resonator such that  $R'_1 = L = -R_2 > 0$ . Skew rays reentrant after 4 reflections and corresponding to Fig. 16. Orthographic projections of the resonator: (a) side view, (b) front view, (c) top view.

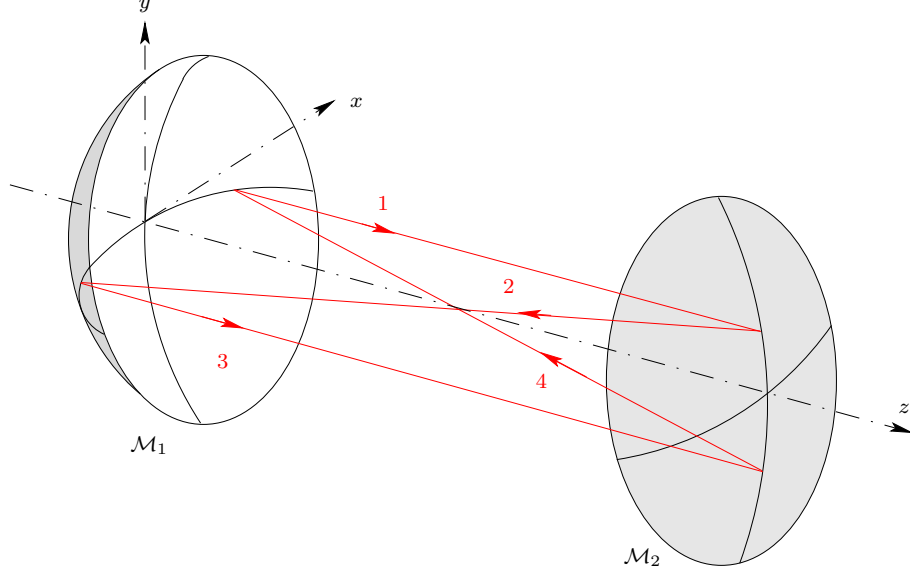


Figure 18: Reentrant skew rays after 4 reflections, corresponding to Fig. 17. Oblique projection.

## 5.2 Another example

We consider the resonator of Sect. 4.2, for which  $R'_1 = 2L = -R_2 = R'_2 > 0$  (it is also the resonator of Sect. 4.1.3); then  $\alpha = \pi/3$ , and every ray is reentrant after 6 reflections. Parameters  $\varepsilon_1$  and  $\varepsilon_2$  and definitions of scaled variables are those of Sect. 4.2.3 and Table 1.

Once more, the initial point ( $M_1$ ) is  $(x_1, 0)$  with  $x_1 = R'_1/4 = L/2$ . We choose  $\theta_{n1} = 10^\circ$  and

$$\xi_1 = \cos \theta_{\xi 1} = \frac{1}{2} \sin \theta_{n1}, \quad \eta_1 = \cos \theta_{\eta 1} = \frac{\sqrt{3}}{2} \sin \theta_{n1}, \quad (60)$$

which means that the projection of the vector  $\mathbf{e}_{n1}$  onto the plane  $(\mathbf{e}_{\xi 1}, \mathbf{e}_{\eta 1})$  makes an angle of  $60^\circ$  with the vector  $\mathbf{e}_{\xi 1}$ . (We have  $\cos^2 \theta_{\xi 1} + \cos^2 \theta_{\eta 1} + \cos^2 \theta_{n1} = 1$ .)

General parameters and initial data are given in Table 3. Parameters in the  $\rho_x$ - $\phi_x$  scaled subspace are given in Table 4 and those in the  $\rho_y$ - $\phi_y$  subspace in Table 5. Results are illustrated by Figs. 19, 20 and 21.

Parameter	Definition	Numerical value
$\alpha$	$\cot^2 \alpha = J > 0$	$\pi/3$
$\varepsilon_1$	$\frac{L}{R'_1 - L} \cot \alpha = \cot \alpha$	0.577 350
$\varepsilon_2$	$\frac{L}{R_2 + L} \cot \alpha = -\cot \alpha$	-0.577 350
$x_1$		$R'_1/4$
$y_1$		0
$\theta_{n1}$		$10^\circ$
$\mathbf{r}_1$	$(x_1, 0)$	$(R'_1/4, 0)$
$\Phi_1$	$(\xi_1, \eta_1) = \left( \frac{1}{2} \sin \theta_{n1}, \frac{\sqrt{3}}{2} \sin \theta_{n1} \right)$	(0.150 384, 0.086 824)

Table 3: Initial numerical values for a skew ray reentrant after 6 reflections.

Parameter	Definition	Numerical value
$\rho_{1x}$	$\frac{1}{\sqrt{\varepsilon_1}} \frac{x_1}{\sqrt{\lambda R'_1}} = \frac{1}{4\sqrt{\varepsilon_1}} \sqrt{\frac{R'_1}{\lambda}}$	$0.329\,019 \sqrt{\frac{R'_1}{\lambda}}$
$\phi_{1x}$	$\sqrt{\varepsilon_1} \sqrt{\frac{R'_1}{\lambda}} \frac{1}{2} \sin \theta_{n1}$	$0.065\,972 \sqrt{\frac{R'_1}{\lambda}}$
$\Delta_x/2$	$\sqrt{(\rho_{1x})^2 + (\phi_{1x})^2}$	$0.335\,567 \sqrt{\frac{R'_1}{\lambda}}$
$\psi_{1x}$	$\tan \psi_{1x} = \frac{\phi_{1x}}{\rho_{1x}}$	$11.338\,117^\circ$

Table 4: Initial numerical values of scaled coordinates in the  $\rho_x$ - $\phi_x$  subspace, for a skew ray reentrant after 6 reflections.

Parameter	Definition	Numerical value
$\rho_{1y}$	$\frac{1}{\sqrt{\varepsilon_1}} \frac{y_1}{\sqrt{\lambda R'_1}}$	0
$\phi_{1y}$	$\sqrt{\varepsilon_1} \sqrt{\frac{R'_1}{\lambda}} \frac{\sqrt{3}}{2} \sin \theta_{n1}$	$0.114\,267 \sqrt{\frac{R'_1}{\lambda}}$
$\Delta_y/2$	$\sqrt{(\rho_{1y})^2 + (\phi_{1y})^2}$	$0.114\,267 \sqrt{\frac{R'_1}{\lambda}}$
$\psi_{1y}$	$\tan \psi_{1y} = \frac{\phi_{1y}}{\rho_{1y}}$	$90^\circ$

Table 5: Initial numerical values of scaled coordinates in the  $\rho_y$ - $\phi_y$  subspace, for a skew ray reentrant after 6 reflections.

$j$	$\psi_{jx}$	$\frac{x_j}{\Delta_x}$	$x_j$
1	$11.338\,117^\circ$	1	$0.25 R'_1$
2	$-48.661\,883^\circ$	0.673 648	$0.168\,412 R'_1$
3	$-108.661\,883^\circ$	-0.326 352	$-0.081\,588 R'_1$
4	$-168.661\,883^\circ$	1	$-0.25 R'_1$
5	$131.338\,117^\circ$	-0.673 648	$-0.168\,412 R'_1$
6	$71.338\,117^\circ$	0.326 352	$0.081\,588 R'_1$

Table 6: Successive coordinates  $x_j$  for a skew ray reentrant after 6 reflections.

$j$	$\psi_{jy}$	$\frac{y_j}{\Delta_y}$	$y_j$
1	$90^\circ$	0	0
2	$30^\circ$	0.866 025	$0.098\,958 R'_1$
3	$-30^\circ$	0.866 025	$0.098\,958 R'_1$
4	$-90^\circ$	0	0
5	$-150^\circ$	-0.866 025	$-0.098\,958 R'_1$
6	$150^\circ$	-0.866 025	$-0.098\,958 R'_1$

Table 7: Successive coordinates  $y_j$  for a skew ray reentrant after 6 reflections.

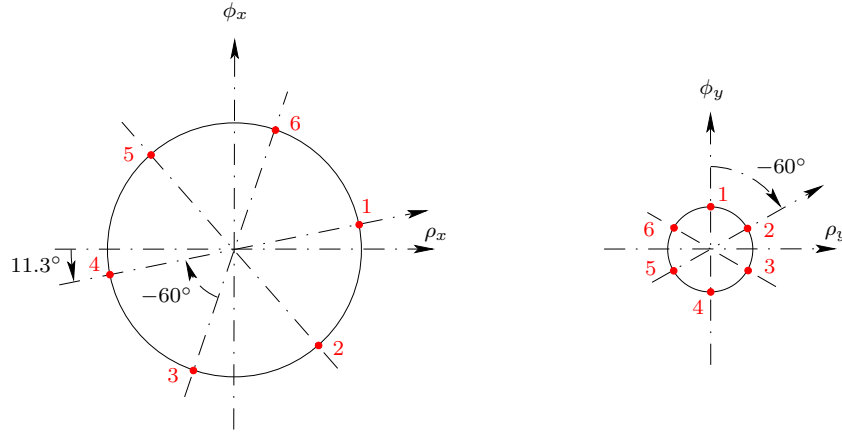


Figure 19: Skew ray reentrant after 6 reflections. Representative points of successive rays in the scaled phase-space. Left: the radius of the circle is  $0.335\,567\sqrt{R'_1/\lambda}$ . Right: the circle radius is  $0.114\,267\sqrt{R'_1/\lambda}$ .

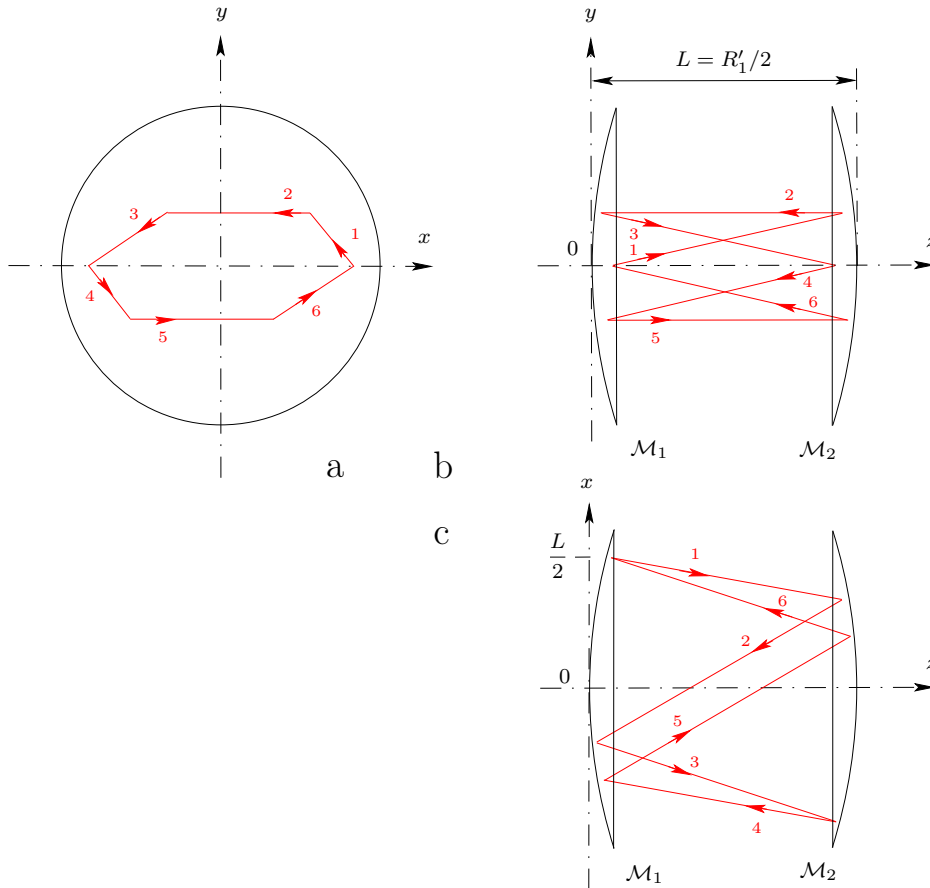


Figure 20: Resonator such that  $R'_1 = 2L = -R_2 = R'_2 > 0$ . Skew rays reentrant after 6 reflections. Orthographic projections of the resonator: (a) side view, (b) front view, (c) top view.



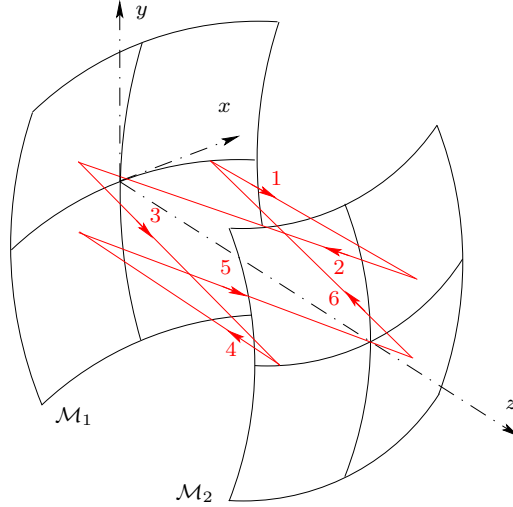


Figure 21: Resonator of Fig. 20. Skew rays reentrant after 6 reflections. Oblique projection.

## 6 Ray tracing in unstable resonators

### 6.1 Meridional rays in unstable resonators

#### 6.1.1 A numerical example

We now provide numerical results obtained by applying our method, based on the Wigner representation of an optical field, the considered resonator being such that  $-R'_1 = L = R_2 > 0$ . The arrangement of vertices and curvature centers of mirrors  $\mathcal{M}_1$  and  $\mathcal{M}_2$  is  $(C_1, \Omega_1, \Omega_2, C_2)$  and the resonator is unstable. Then

$$\cot^2 \alpha = J = \frac{(R'_1 - L)(L + R_2)}{L(L - R'_1 + R_2)} = -\frac{4}{3} < -1. \quad (61)$$

and  $\alpha = i\beta$ . Since  $\beta L > 0$  ( $L > 0$ ), we obtain  $\beta = 1.316958$  and  $\coth \beta = 2/\sqrt{3}$ . We also have

$$\cos^2 \alpha = \left(1 - \frac{L}{R'_1}\right) \left(1 + \frac{L}{R_2}\right) = 4, \quad (62)$$

and since  $\beta > 0$ , we have  $\cosh \beta = 2$  and  $\sinh \beta = \sqrt{3}$ . Moreover, since  $R'_1(R'_1 - L) = 2L^2 > 0$ , we have  $\mathfrak{s} = 1$ , so that

$$\chi_1 = \frac{L}{R'_1 - L} \coth \beta = -\frac{1}{\sqrt{3}} = -0.577350, \quad \chi_1 R'_1 > 0, \quad (63)$$

and

$$\chi_2 = \frac{L}{R_2 + L} \coth \beta = \frac{1}{\sqrt{3}} = 0.577350, \quad \chi_2 R_2 > 0. \quad (64)$$

Since in this example we consider meridional rays in the  $x$ - $z$  plane, we only use the following scaled coordinates

$$\rho_x = \frac{1}{\sqrt{|\chi_1|}} \frac{x}{\sqrt{\lambda L}}, \quad (65)$$

$$\phi_x = \sqrt{|\chi_1|} \sqrt{\frac{L}{\lambda}} \sin \theta_n. \quad (66)$$

Parameter	Definition	Numerical value
$\alpha$	$\cot^2 \alpha = J$	$-4/3$
$\beta$	$-\mathrm{i}\alpha$	1.316 958
$\coth \beta$		$2/\sqrt{3}$
$\cosh \beta$		2
$\sinh \beta$		$\sqrt{3}$
$\chi_1$	$\frac{L}{R'_1 - L} \coth \beta$	$-0.577\ 350$
$\chi_2$	$\frac{L}{R_2 + L} \coth \beta$	0.577 350
$N$		75
$x_1$	$L/N$	$L/75 = 0.013\ 333\ L$
$\theta_{n1}$		$0^\circ$
$\mathbf{r}_1$	$(x_1, 0)$	$(L/75, 0) = (0.013\ 333\ L, 0)$
$\Phi_1$	$(\xi_1, \eta_1) = (\sin \theta_{n1}, 0)$	$(0, 0)$
$\rho_{1x}$	$\frac{1}{\sqrt{ \chi_1 }} \frac{x_1}{\sqrt{\lambda L}} = \frac{1}{N\sqrt{ \chi_1 }} \sqrt{\frac{L}{\lambda}}$	$1.316\ 074 \frac{1}{N} \sqrt{\frac{L}{\lambda}}$
$\phi_{1x}$	$\sqrt{ \chi_1 } \sqrt{\frac{L}{\lambda}} \sin \theta_{n1}$	0
$A_x$	$(\rho_{1x})^2 - (\phi_{1x})^2$	$1.732\ 051 \frac{L}{N^2 \lambda}$

Table 8: Numerical values of parameters and of initial data for ray tracing in an unstable resonator such that  $-R'_1 = L = -R_2 > 0$ .

We may then draw up Table 8, rather similar to Table 1.

In the 2-dimensional subspace of the scaled phase-space, successive points  $(\rho_{jx}, \phi_{jx})$  are on the hyperbole whose equation is

$$(\rho_x)^2 - (\phi_x)^2 = A_x, \quad (67)$$

where  $A_x$  is given by the initial ray to be considered:  $A_x = (\rho_{1x})^2 - (\phi_{1x})^2$ . Successive points are obtained according to the recurrence

$$\begin{pmatrix} \rho_{(j+1)x} \\ \phi_{(j+1)x} \end{pmatrix} = \begin{pmatrix} \cosh \beta & \sinh \beta \\ \sinh \beta & \cosh \beta \end{pmatrix} \begin{pmatrix} \rho_{jx} \\ \phi_{jx} \end{pmatrix}. \quad (68)$$

The initial ray (ray 1, that is, after one reflection on  $\mathcal{M}_1$ ) is defined by

$$x_1 = \frac{L}{N}, \quad N = 75, \quad (69)$$

and

$$\theta_{n1} = 0^\circ, \quad (70)$$

which means that ray 1 is perpendicular to  $\mathcal{M}_1$ . The corresponding scaled coordinates are

$$\rho_{1x} = \frac{1}{\sqrt{|\chi_1|}} \frac{x_1}{\sqrt{\lambda L}} = \frac{1}{N\sqrt{|\chi_1|}} \sqrt{\frac{L}{\lambda}}, \quad (71)$$

$$\phi_{1x} = \sqrt{|\chi_1|} \sqrt{\frac{L}{\lambda}} \sin \theta_{n1} = 0. \quad (72)$$

Finally  $x_j$  is deduced from  $\rho_{jx}$  by using

$$x_j = x_1 \frac{\rho_{jx}}{\rho_{1x}} = \frac{L}{N} \frac{\rho_{jx}}{\rho_{1x}}. \quad (73)$$

The first successive iterations are given in Table 9. Figure 22 shows representative points of successive rays in the  $\rho_x$ - $\phi_x$  plane, according to Table 9, and Fig. 23 shows the corresponding rays in the physical space (section of the resonator in the  $x$ - $z$  plane). The results are in accordance with those of Fig. II.3 (Part II).

$j$	$\frac{\rho_{jx}}{\sqrt{A_x}}$	$\frac{\phi_{jx}}{\sqrt{A_x}}$	$x_j$
1	1	0	$L/75$
2	2	$\sqrt{3}$	$2L/75$
3	7	$4\sqrt{3}$	$7L/75$
4	26	$15\sqrt{3}$	$26L/75$
5	97	$56\sqrt{3}$	$97L/75$

Table 9: Successive coordinates of a meridional ray in an unstable resonator. Data correspond to Table 8.

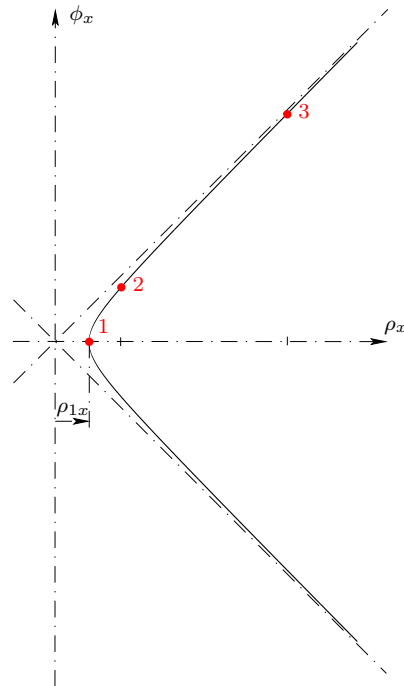


Figure 22: Unstable resonator: representative points of successive rays in the scaled phase-space, according to Table 9.

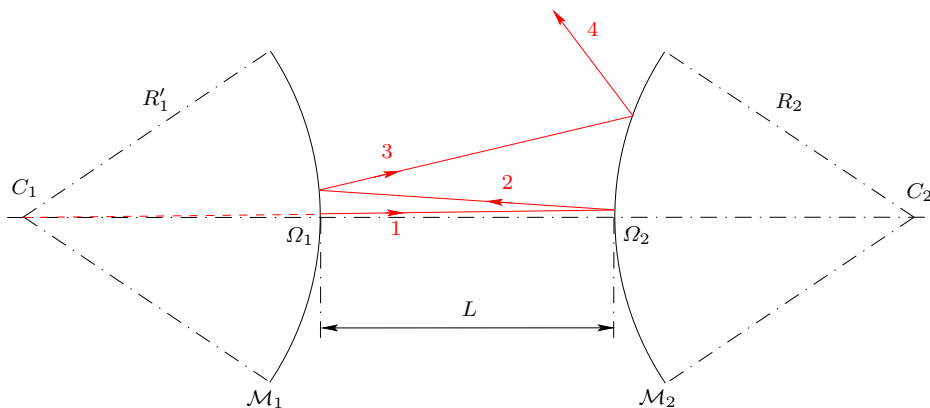


Figure 23: Meridional rays in an unstable resonator corresponding to Table 9 and Fig. 22. We have  $-R'_1 = L = R_2 > 0$ . The initial ray is such that  $x_1 = L/75$ .

### 6.1.2 Other examples

We provide now two examples which can be dealt with by using paraxial geometrical optics, as done in Sect. 4.1, and which are as follows.

- Figure 24. The arrangement of curvature centers and vertices is  $(\Omega_1, C_1, C_2, \Omega_2)$ : the resonator is unstable and  $\alpha = i\beta$ ,  $\beta > 0$ . The resonator is symmetrical with  $R'_1 = R'_2 > 0$ . Since  $L > R'_1$ , we have  $R'_1(R'_1 - L) < 0$  and  $\varepsilon = -1$ . The situation is that of Fig. II.4. The rays are alternatively diverging, that is, every ray crosses the optical axis after reflection.
- Figure 25. The resonator is confocal (not symmetrical) and the arrangement of curvature centers and vertices is  $(\Omega_1, C_2, \Omega_2, C_1)$ : the resonator is unstable and  $\alpha = (\pi/2) + i\beta$ . The situation is that of Fig. II.5. The rays are semi-alternatively diverging: one ray of two crosses the optical axis after reflection.

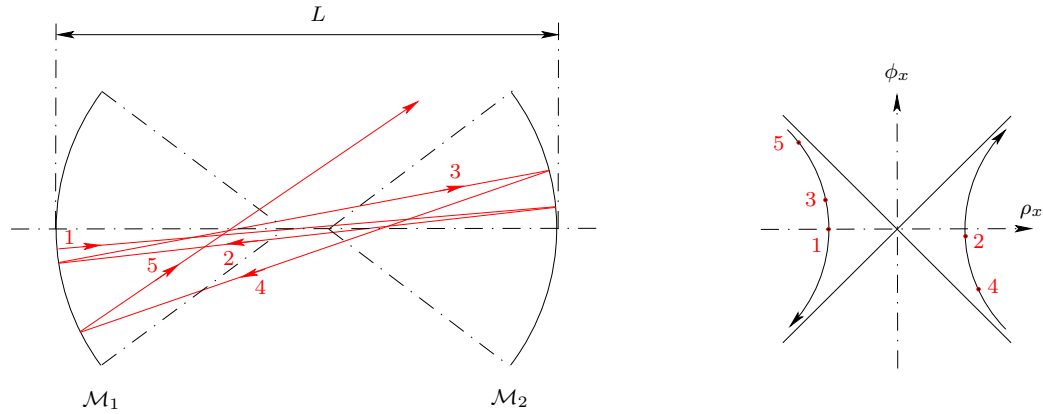


Figure 24: Ray tracing in an unstable resonator. Here  $R'_1 = -R_1 = -R_2 > 0$  and  $\varepsilon = -1$ . Rays are alternatively divergent.

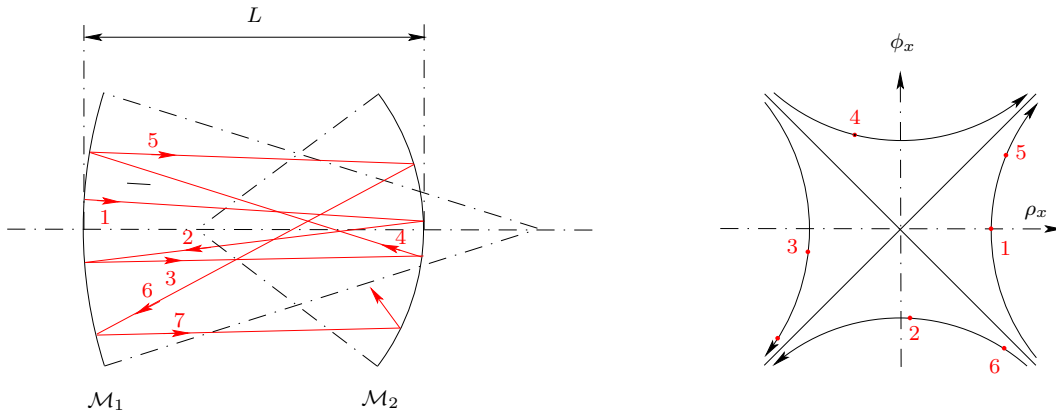


Figure 25: Ray tracing in an unstable confocal resonator. Rays are semi-alternatively divergent.

## 6.2 Skew rays in an unstable resonator

We consider an unstable resonator with  $-R'_1 = 2L = R_2 > 0$ . Then

$$\cot^2 \alpha = J = \frac{(R'_1 - L)(L + R_2)}{L(L - R'_1 + R_2)} = -\frac{9}{5} < -1, \quad (74)$$

and  $\alpha = i\beta$ . Since  $\beta L > 0$  ( $L > 0$ ), we obtain  $\beta = 0.962\,424$ ,  $\coth \beta = 1.5$  and  $\sinh \beta = 1.118\,034$ . We also have  $R'_1(R'_1 - L) > 0$  and  $\mathfrak{s} = 1$ .

The initial ray (ray 1) is chosen such that

$$\mathbf{r}_1 = (x_1, y_1) = (-L/N, 0), \quad N = 100, \quad (75)$$

$$\Phi_1 = (\cos \theta_{\xi 1}, \cos \theta_{\eta 1}) = \left( \frac{1}{2} \sin \theta_{n1}, -\frac{\sqrt{3}}{2} \sin \theta_{n1} \right), \quad \theta_{n1} = -5^\circ. \quad (76)$$

Fractional parameters and initial values are given in Table 10.

Parameter	Definition	Numerical value
$\alpha$	$\cot^2 \alpha = J$	$-9/5$
$\beta$	$-i\alpha$	$0.962\,424$
$\coth \beta$		$3/\sqrt{5} = 1.341\,641$
$\cosh \beta$		$1.500\,000$
$\sinh \beta$		$1.118\,034$
$\chi_1$	$\frac{L}{R'_1 - L} \coth \beta$	$-0.447\,214$
$\chi_2$	$\frac{L}{R_2 + L} \coth \beta$	$0.447\,214$
$N$		$100$
$x_1$	$-L/N$	$-L/100 = -0.010\,000\,L$
$y_1$		$0$
$\theta_{n1}$		$-5^\circ$
$\mathbf{r}_1$	$(x_1, 0)$	$(-L/100, 0) = (-0.010\,000\,L, 0)$
$\Phi_1$	$\left( \frac{1}{2} \sin \theta_{n1}, -\frac{\sqrt{3}}{2} \sin \theta_{n1} \right)$	$(-0.043\,578, 0.075\,479)$

Table 10: Numerical values of parameters and of initial data for skew-ray tracing in an unstable resonator such that  $-R'_1 = L = -R_2 > 0$ .

The recurrence for  $\rho_x$  and  $\phi_x$  is given by

$$\begin{pmatrix} \rho_{(j+1)x} \\ \phi_{(j+1)x} \end{pmatrix} = \begin{pmatrix} \cosh \beta & \sinh \beta \\ \sinh \beta & \cosh \beta \end{pmatrix} \begin{pmatrix} \rho_{jx} \\ \phi_{jx} \end{pmatrix} = \begin{pmatrix} 1.500\,000 & 1.118\,034 \\ 1.118\,034 & 1.500\,000 \end{pmatrix} \begin{pmatrix} \rho_{jx} \\ \phi_{jx} \end{pmatrix}, \quad (77)$$

and the recurrence for  $\rho_y$  and  $\phi_y$  involves the same matrix.

Initial scaled coordinates are given in Tables 11 and 12; successive coordinates are given in Tables 13 and 14. The results are shown in Fig. 26.

The considered ray is skew, which means that points  $j$  in side view, Fig. 26–a, are not on a straight line. This can be checked by observing that segments 1–2 and 2–3 are not collinear. Also less apparent, this holds true for the other segments, as shown by Table 15, which provides the slopes of successive segments  $j$ – $(j+1)$ .

Parameter	Definition	Numerical value
$\rho_{1x}$	$\frac{1}{\sqrt{ \chi_1 }} \frac{x_1}{\sqrt{\lambda L}} = \frac{-1}{N\sqrt{ \chi_1 }} \sqrt{\frac{L}{\lambda}}$	$-0.029\,907 \sqrt{\frac{L}{\lambda}}$
$\phi_{1x}$	$\frac{1}{2} \sqrt{ \chi_1 } \sqrt{\frac{L}{\lambda}} \sin \theta_{n1}$	$-0.029\,142 \sqrt{\frac{L}{\lambda}}$
$A_x$	$(\rho_{1x})^2 - (\phi_{1x})^2$	$0.045\,154\,8 \times 10^{-3} \frac{L}{\lambda}$

Table 11: Skew rays in an unstable resonator: initial numerical values of scaled coordinates in the  $\rho_x$ - $\phi_x$  subspace.

Parameter	Definition	Numerical value
$\rho_{1y}$	$\frac{1}{\sqrt{ \chi_1 }} \frac{y_1}{\sqrt{\lambda L}}$	0
$\phi_{1y}$	$-\frac{\sqrt{3}}{2} \sqrt{ \chi_1 } \sqrt{\frac{L}{\lambda}} \sin \theta_{n1}$	$0.050\,476 \sqrt{\frac{L}{\lambda}}$
$A_y$	$(\rho_{1y})^2 - (\phi_{1y})^2$	$-2.548\,266 \times 10^{-3} \frac{L}{\lambda}$

Table 12: Skew rays in an unstable resonator: initial numerical values of scaled coordinates in the  $\rho_y$ - $\phi_y$  subspace.

$j$	$\frac{\rho_{xj}}{\sqrt{L/\lambda}}$	$\frac{\phi_{xj}}{\sqrt{L/\lambda}}$	$x_j$	$j$	$\frac{\rho_{yj}}{\sqrt{L/\lambda}}$	$\frac{\phi_{yj}}{\sqrt{L/\lambda}}$	$y_j$
1	-0.029 907	-0.029 142	-0.02 $L$	1	0	0.050 476	0
2	-0.077 443	-0.077 150	-0.051 789 $L$	2	0.056 434	0.075 714	0.037 741 $L$
3	-0.202 421	-0.202 309	-0.135 367 $L$	3	0.169 302	0.176 666	0.113 223 $L$
4	-0.529 819	-0.529 777	-0.354 311 $L$	4	0.451 472	0.454 284	0.301 927 $L$
5	-1.387 037	-1.387 021	-0.927 568 $L$	5	1.185 113	1, 186 187	0.792 557 $L$

Table 13: Successive coordinates  $x_j$  of a skew ray in an unstable resonator. Data correspond to Table 10.

Table 14: Successive coordinates  $y_j$  of a skew ray in an unstable resonator. Data correspond to Table 10.

$j$	1	2	3	4
Segment	1-2	2-3	3-4	4-5
$\frac{y_{j+1} - y_j}{x_{j+1} - x_j}$	-1.187	-0.903	-0.862	-0.856

Table 15: Slopes of segments  $j$ - $(j+1)$  of Fig. 26-a.

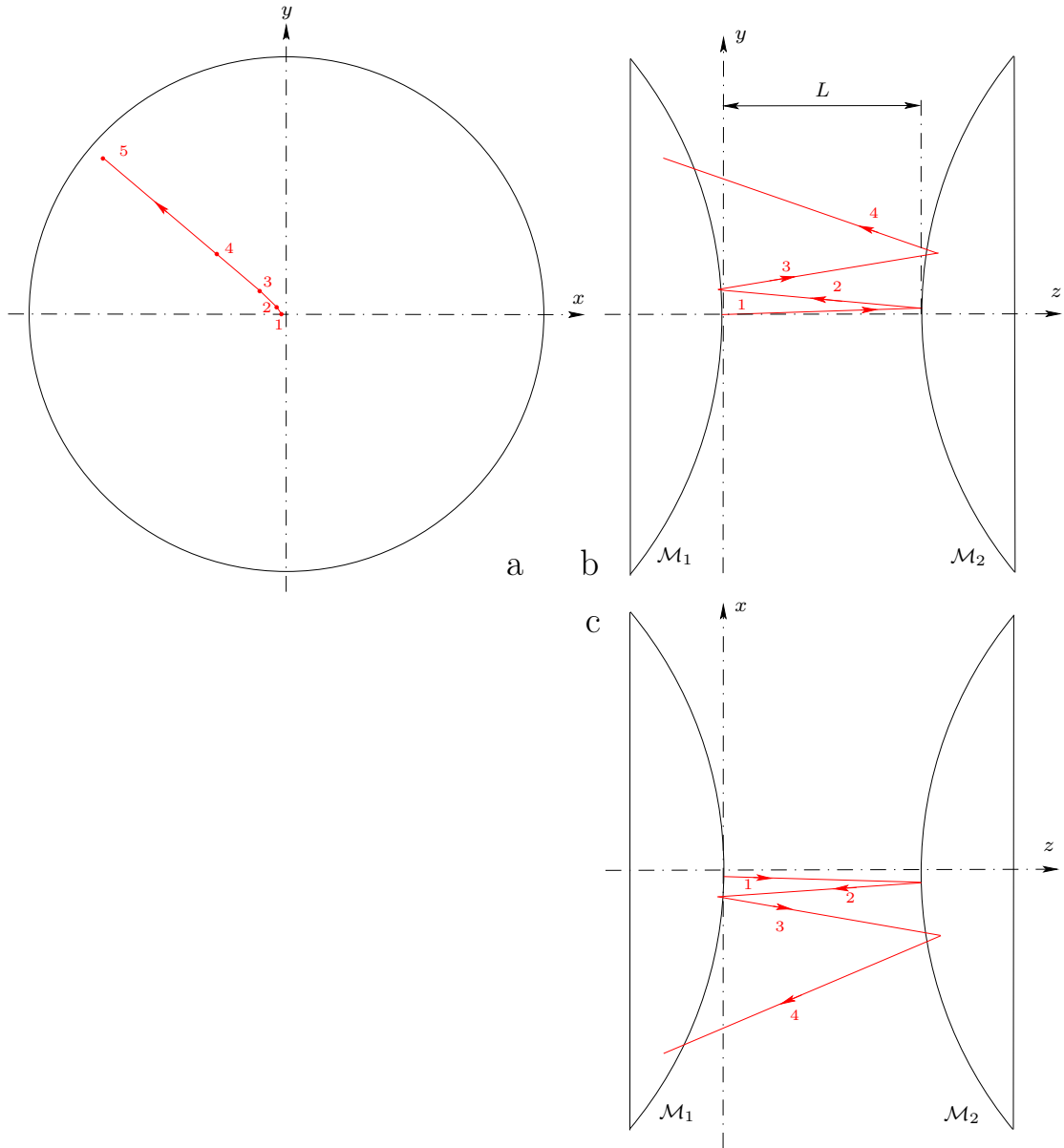


Figure 26: Skew rays in an unstable resonator for which  $-R_1' = 2L = R_2 > 0$ . Orthographic projections of the resonator: (a) side view, (b) front view, (c) top view.

## 7 Conclusion

Optical resonators may be classified according to their stability, which depends on the arrangement, on the optical axes, of vertices and curvature centers of their mirrors [4, 5]. The previous analysis of rays in optical resonators leads us to an additional classification. Reentrant rays exist only in stable resonators, whose associated fractional-orders are real numbers. On the other hand, fractional orders associated with unstable resonators take the form  $\alpha = i\beta$  or  $\alpha = i\beta \pm (\pi/2)$ , and the ways the rays diverge are distinct in both cases. When  $\alpha = i\beta$ , we may define two subclasses, according to the sign of  $R'_1(R'_1 - L)$ . The resulting classification is given in Table 16 and is as follows.

- Class I: Stable resonators. The arrangement of vertices and curvature centers on the optical axis is  $(\Omega_1, \Omega_2, C_1, C_2)$  up to circular permutation. The index arrangement is 1212 or 2121.
- Class II: Unstable resonators, simply divergent or alternatively divergent. The arrangement of vertices and centers is  $(\Omega_1, \Omega_2, C_2, C_1)$  up to circular permutation. The index arrangement is 1122 up to circular permutation. Curvature centers are adjacent; or vertices are adjacent.
- Class III: Unstable resonators, semi-alternatively divergent. The arrangement of vertices and centers is  $(\Omega_1, C_2, \Omega_2, C_1)$  up to circular permutation. The index arrangement is 1122 up to circular permutations. On the optical axis, curvature centers alternate with vertices.

Class	Arrangement	Indices	$\alpha$	Stability	$\mathfrak{s}$	Rays
I	$(\Omega_1, \Omega_2, C_1, C_2)$	1212	real	stable		reentrant if $\alpha = m\pi/q$
I	$(C_2, \Omega_1, \Omega_2, C_1)$	2121	real	stable		reentrant if $\alpha = m\pi/q$
I	$(C_1, C_2, \Omega_1, \Omega_2)$	1212	real	stable		reentrant if $\alpha = m\pi/q$
I	$(\Omega_2, C_1, C_2, \Omega_1)$	2121	real	stable		reentrant if $\alpha = m\pi/q$
II	$(\Omega_1, \Omega_2, C_2, C_1)$	1221	$i\beta$	unstable	1	simply divergent
II	$(C_1, \Omega_1, \Omega_2, C_2)$	1122	$i\beta$	unstable	1	simply divergent
II	$(C_2, C_1, \Omega_1, \Omega_2)$	2112	$i\beta$	unstable	1	simply divergent
II	$(\Omega_2, C_2, C_1, \Omega_1)$	2211	$i\beta$	unstable	-1	alternatively divergent
III	$(\Omega_1, C_2, \Omega_2, C_1)$	1221	$i\beta \pm (\pi/2)$	unstable		semi-alternatively divergent
III	$(C_1, \Omega_1, C_2, \Omega_2)$	1122	$i\beta \pm (\pi/2)$	unstable		semi-alternatively divergent
III	$(\Omega_2, C_1, \Omega_1, C_2)$	2112	$i\beta \pm (\pi/2)$	unstable		semi-alternatively divergent
III	$(C_2, \Omega_2, C_1, \Omega_1)$	2211	$i\beta \pm (\pi/2)$	unstable		semi-alternatively divergent

Table 16: Resonator classification. The vertex of mirror  $\mathcal{M}_1$  is  $\Omega_1$  and  $C_1$  is its center of curvature. They are  $\Omega_2$  and  $C_2$  for  $\mathcal{M}_2$ . Every arrangement can also be read from right to left, without changing the properties of the corresponding resonator. The parameter  $\mathfrak{s}$  denotes the sign of  $R'_1(R'_1 - L)$ , where  $L$  denotes the resonator length and  $R'_1$  the curvature radius of  $\mathcal{M}_1$ .

The method of ray tracing, described in this article, may be the subject of further developments. It can be applied, for example, to resonators made up of toric mirrors, that is, mirrors having two principal curvatures at their vertices. Assuming that principal sections are in the plane  $x-z$  and  $y-z$  for both mirrors, such a resonator can be analyzed as a stable resonator, for instance in the  $x-z$  section, and as an unstable resonator in the  $y-z$  section. In the  $x-z$  section, ray representative points in the 2-dimension scaled subspace  $\rho_x-\phi_x$  are on a circle; while in the 2-dimension scaled subspace  $\rho_y-\phi_y$  they lie on a hyperbole. Globally, the resonator is unstable, because rays other than those lying in the  $x-z$  plane are divergent.

Finally we point out that simulations of reentrant rays in optical resonators can be performed with usual ray-tracing softwares (e.g. such as Zeemax [6]). Reentrant rays in stable resonators afford some advantages for maintaining polarization states at laser outputs [7], or for reducing cavity lengths of some lasers [7-9].



## References

- [1] P. Pellat-Finet, É. Fogret, “Effect of Diffraction on Wigner Distributions of Optical Fields and how to Use It in Optical Resonator Theory. I – Stable Resonators and Gaussian Beams,” arXiv 2005.13430v1 (2020) 1–20. (2nd version: 2005.13430v2.)
- [2] P. Pellat-Finet, É. Fogret, “Effect of Diffraction on Wigner Distributions of Optical Fields and how to Use It in Optical Resonator Theory. II – Unstable Resonators,” arXiv 2203.14546v1 (2022) 1–25.
- [3] P. Pellat-Finet, É. Fogret, “Ray tracing based on the Wigner representation of optical fields,” *Óptica Pura y Aplicada* **51** (2018) 49025:1-10.
- [4] P. Pellat-Finet, *Optique de Fourier. Théorie métaxiale et fractionnaire*, Springer, Paris, 2009.
- [5] P. Pellat-Finet, É. Fogret, “Fractional Fourier optics theory of optical resonators,” in: P. S. Emerson (Ed.), *Progress in optical fibers*, Nova Science Publishers, New York (2011) 299–351.
- [6] F. H. Tseng, S. K. Liu, “Simulation of multi-reentrant two-mirror ring cavity lasers,” *Proc. SPIE* **6834** (2008) 46:1–12.
- [7] S. L. Huang, Y. H. Chen, P. L. Huang, J. Y. Yi, H. Z. Cheng, “Multi-reentrant nonplanar ring laser cavity,” *IEEE J. Quantum Electron.* **38** (2002) 1301–1308.
- [8] A. Sennaroglu, A. M. Kowalevich, E. P. Ippen, J. G. Fujimoto, “Compact femtosecond lasers based on novel multipass cavities,” *IEEE J. Quantum Electron.* **40** (2004) 519–528.
- [9] J. Y. Yi, L. H. Chen, S. L. Huang, “Efficient and compact Yb:YAG ring laser,” *IEEE J. Quantum Electron.* **42** (2006) 791–796.